De Novo Proteins Adopt Catalytic Function

A Capstone Project Submitted in Partial Fulfillment of the
Requirements of the Renée Crown University Honors Program at
Syracuse University

Cara Chester

Candidate for Bachelor of Science in Biochemistry
and Renée Crown University Honors
Spring 2020

Honors Capstone Project in Biochemistry

Thesis Advisor: _____
Olga Makhlynets, PhD

Thesis Reader: _____
Ivan Korendovych, PhD

Honors Director: _____
Dr. Danielle Smith, Director

Abstract

Enzymes often require metallocofactors and utilize radicals in order to facilitate complex chemical reactions. The inherent complexity of these metalloproteins makes it difficult to determine the mechanisms that underlie their reactivity. The DeGrado lab made use of Due Ferri (DF) helical bundles to design model proteins that replicate coordination geometry and interactions of non-heme diiron enzymes in hopes that these proteins, with lower overall complexity, can provide insight into the structure and function of metalloenzymes. Model systems have been used to investigate the mechanisms used by proteins to stabilize radicals and prevent harmful side reactions. Recently, the DeGrado lab showed that a zinc complexed DFsc derived protein stabilizes a semiquinone radical.

The Makhlynets lab wanted to explore the contribution of metal in radical stabilization. In order to do so, UFsc, a single metal ion-binding protein, and 4G-UFsc, a mutant of UFsc created by introducing 4 mutations to widen the channel that leads to the metal center, were created. Based on results, the Makhlynets lab discovered that one metal ion is sufficient to fulfill the radical stabilization role in these designed *de novo* proteins. Mutations were then introduced to the binding pocket of UFsc and 4G-UFsc in order to establish coordination geometry. Experiments were run with various metals to identify whether ligand-metal coordination of these *de novo* proteins is dependent on the metal. In this work, we propose that the DFsc/UFsc family of proteins can be used as a model to study the mechanisms of metalloenzymes.

Executive Summary

A protein adopts many different functions in nature. This variability of proteins is due to nature's ability to modify function through structural changes, or by exquisitely orienting side chains on a protein backbone to coordinate various ligands (metals, organic molecules, and other cofactors) to confer chemical reactivity[1,2]. *De novo* design proteins, which are made from scratch (De novo is Latin for "anew"), are used in the field to understand how nature fine tunes active sites of enzymes for specific chemical reactions. The DeGrado lab pioneered the use of Due Ferri helical bundles, which were designed to replicate the coordination geometry and interactions of non-heme diiron enzymes[2]. The Due Ferri family of *de novo* proteins share a similar structure. They are four helix bundle diiron carboxylate proteins.

Our lab, the Makhlynets lab, utilized Due Ferris single chain (DFsc) to understand how four helical bundles bound to metal ions can catalyze complex reactions through mechanisms that are found in nature. DFsc in particular is a very important protein of study because it is one of the DF family proteins that mimics the asymmetry of natural proteins, tightly binding iron to exhibit modest ferroxidase activity (oxidizes iron and facilitates its transfer), an important transformation initiated by ceruloplasmin and ferritin observed in humans[1].

Recently, the DeGrado lab discovered that a DFsc derived protein coordinated with two zinc ions [3His-GZDFsc-Zn_2] can efficiently stabilize a semiquinone radical anion formed by oxidation of 3,5-di-tert-butylcatechol (DTBC)[2]. The goal of this project is to examine the central fundamental principle of how proteins in nature facilitate complex chemical reactions through rational assembly of amino acids. To better understand how these metalloenzymes function in

nature, our lab examined the role of the metal ion in these metalloenzymes, specifically, whether the metal ion is essential for the radical stabilization discovered by the DeGrado lab. The first part of this thesis focuses on evaluating the contribution of metal to radical stabilization. To broaden this evaluation of metal's role in the stabilization of a radical, DFsc was converted into a single metal-binding protein (UFsc). Additionally, our lab introduced 4 mutations to UFsc to widen the channel that leads to the metal binding site, creating 4G-UFsc.

Our lab, the Makhlynets lab, discovered that UFsc and 4G-UFsc promote semiquinone radical formation in the presence of one equivalence of Zn^{2+} and that the radical yield of 4G-UFsc is comparable to that of DFsc[3]. This demonstrates that one metal ion is sufficient to fulfill the radical stabilization role. The second part of this thesis focuses on establishing the coordination geometry in these proteins. This was done by introducing mutations to the binding pockets of UFsc and 4G-UFsc and to examine the effects of these mutations using(ITC) and circular dichroism (CD). Previous experiments showed the location of iron in UFsc. One goal discussed in the second part of this thesis is to identify the location of other metals and identify whether the ligand-metal coordinations are the same for different metals or whether these coordinations are dependent on the metal.

Through our work, we have discovered that UFsc binds transition metals with high affinity and is capable of stabilizing the semiquinone radical anion[3]. By mutating the binding pocket of UFsc and 4G-UFsc, we uncovered information regarding the ligand-metal coordination of the binding pocket and found that all mutations reduced the affinity of proteins to metals but to a different extent.

Future studies are needed to further determine the ligand-metal coordination within the binding pocket of these proteins. More mutants can be synthesized in order to try and determine which residues are essential for metal binding and whether mutations to the pocket can increase the protein's affinity for metal ions. After the creation of mutants, the next step is to test different ligands.

Table of Contents:

List of Illustrative Material

Figures

Tables

Acknowledgements

First, I would like to thank my advisor, Dr. Olga Makhlynets, for providing me with the opportunity to conduct research as an undergraduate student. I am grateful for your help and support over the past few years. Thank you for creating a class that gave students the opportunity to participate in a research lab through CHE 119. I am also thankful for Dr. Ivan Korendovych for being a reader of this thesis and providing valuable feedback and support during lab meetings.

I would also like to extend my sincere gratitude to Dr. Areetha D'Souza for all of her guidance, support, and encouragement over the course of my time in the Makhlynets lab. I would also like to thank Alona Kelusha and Jennifer Yoon for their support and for sharing their knowledge and expertise with me.

To all of the members of the Makhlynets/Korendovych lab, thank you for the support over the years. I have truly enjoyed the friendships and will take the knowledge and advice given to me on my next endeavors.

Lastly, I would like to thank my family and friends for your consistent encouragement and support during my studies at Syracuse University.

Chapter 1: Expression and Purification of DFsc/UFsc Family of Proteins

1.1. Introduction

The variability of proteins to function as enzymes, facilitating complex chemical reactions with high selectivity and efficiency, is due to nature's ability to modify function through structural changes, or by exquisitely orienting side chains on a protein backbone to coordinate various ligands (metals, organic molecules, and other cofactors) to confer chemical reactivity[1–3]. Highly reactive radicals that can be toxic to the human body can be utilized by enzymes to promote reactions that are essential for life. For many of these enzymes, metallofactors are required to generate radicals. For example, urease is a naturally found enzyme that utilizes two nickel ions to mediate the hydrolysis of urea to produce ammonia and carbon dioxide[4]. Urease is roughly 500 kDa by mass and is composed of many subunits[5]. In nature, the proteins that catalyze these complex chemical reactions are very large, intricate molecules making it difficult to determine the mechanisms and reactivity of radical-promoting enzymes.

De novo is Latin for "anew" and *de novo* designed proteins that are made from scratch are used in the field to explore how nature fine tunes such active sites of enzymes for specific chemical reactions[3]. *De novo* design lets us examine these large enzymes, and the reactions that they facilitate on a much simpler level. These designed monomer proteins can facilitate the same complex reactions as the intricate enzymes found in nature and by scaling the size of the proteins down to a much simpler level, we can examine the central fundamental principle of how proteins in nature facilitate complex reactions through rational assembly of amino acids.

The DeGrado lab developed Due Ferri (DF) helical bundles designed to imitate the coordination geometry and interactions of naturally existing non-heme diiron enzymes[6]. The DF family of *de novo* proteins all share a similar structure of a four-helix diiron carboxylate protein. When bound to metal ions, DF family proteins can facilitate multiple chemical transformations. Model systems, such as the DF family proteins, are being used to investigate the mechanisms used by proteins (such as urease) to stabilize radicals and prevent harmful side reactions[3].

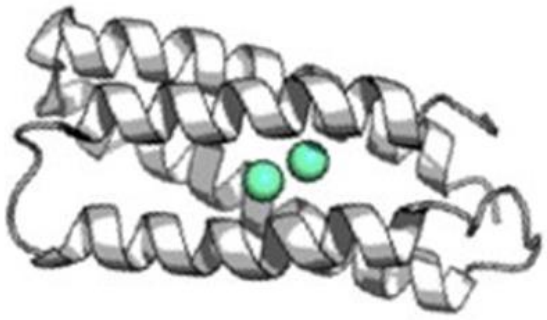

Figure 1. The structure of the Due Ferri (DF) de novo proteins: four helical bundles bound to metal ions.

The DF family of de novo proteins includes Due Ferri single chain (DFsc). The catalytic center of DFsc, two iron atoms coordinated by two histidine (His) amino acids and four carboxylates from glutamate (Glu) residues, is located in a four-helix bundle[7]. DFsc has a motif similar to that of urease, as urease is composed of a reactive site of four histidine amino acids and a carbonyl lysine that bridges the two metals[4]. Experiments set out to establish coordination geometry in DF family proteins resulted in the conclusion that the metal ion is bound to a site composed of His77, Glu44, and Glu74, however, there could be more ligands coordinating to the metal ions[3]. NMR structure of the interaction of DFsc and 3,5-di-tert-

butylcatechol (DTBC) allowed for us to build a structural model of the interaction. In the lowest energy model, the substrate is located inside a hydrophobic pocket lined by 4 alanine residues (Ala10, Ala14, Ala43, and Ala47)[3].

As will be discussed in further detail in the next chapter of this thesis, our group sought out to explore the contribution of metal in these metalloenzymes that allow them to facilitate complex reactions such as radical stabilization. To do so, we converted DFsc into a single metal-binding protein (Uno Ferro single chain, UFsc) by mutating the bridging Glu104 to a histidine. We then created 4G-UFsc by introducing A10G, A14G, A43G, and A47G mutations to widen the channel that leads to the metal center in hopes to improve substrate access[8]. As will be discussed in the last chapter of this thesis, mutations were introduced in UFsc and 4G-UFsc in order to establish coordination geometry in these *de novo* proteins. The mutations introduced are shown below in Table 1.

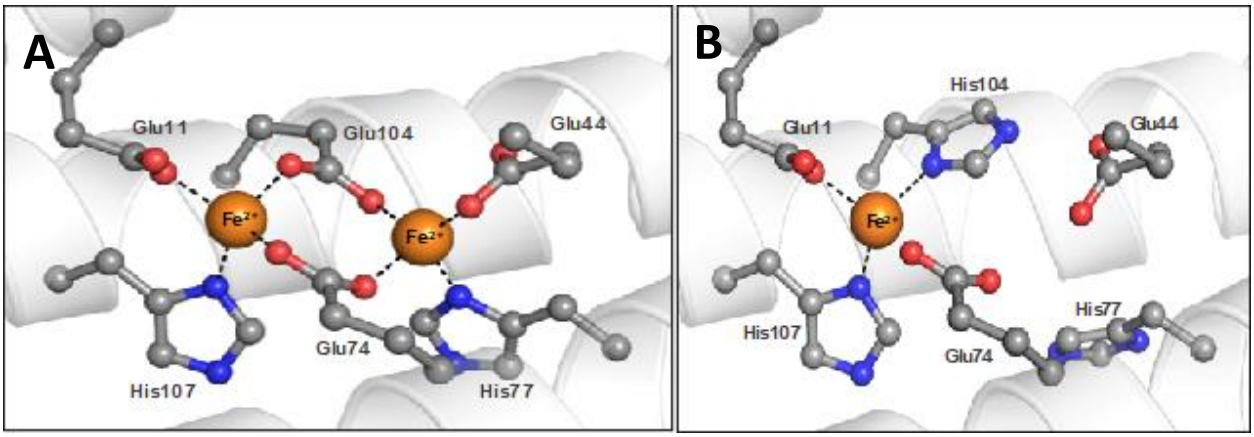

Figure 2. Rosetta (protein crystal structure modeling of PDB code 2HZ8) design of a single point mutation at position 104 to incorporate a histidine ligand (creating a two-His, 1-carboxylate motif) (A) DFsc (B) UFsc.

Table 1. Mutations introduced in UFsc and 4G-UFsc.

UFsc and 4G-UFsc Mutants
E44Q
E44L & Y18F
E11Q
H107Q
E74D
E74H
E74Q

The DFsc/UFsc family of proteins share the same protocol for the protein expression and protein purification process. The protein was stripped of metals, specifically nickel used in our on-resin nickel chromatography purification, using an excess amount of metal-chelator, EDTA. The EDTA treated protein sample was buffer exchanged into a Tris-NaCl buffer solution and dialyzed against the buffer to completely remove the chelator. The DNA sequence that codes for DFsc protein was synthesized and the gene was cloned into pMCSG49 expression vector via ligase independent cloning. Site-directed mutagenesis was performed using customized primers and following standard protocols. For protein expression, the plasmid containing the gene of interest was transformed into *E.coli* BL21(DE3) cells.

Since the focus of this project is on metalloproteins, it was extremely important to ensure our proteins were homogenously pure and free of inorganic contaminants before incorporation of our desired metal during experimentation. Before experimentation could occur protein purification and binding stoichiometry of metal to protein had to be determined

following protein expression and purification. The binding stoichiometry of metal to protein was determined by a cobalt titration experiment and by isothermal titration calorimetry (ITC). Concentration of metal content in our buffer solutions, stock metal solutions, and all proteins were measured using ICP (Inductively Coupled Plasma) analysis.

In our research it is important to be thorough and as precise as possible because any metal or EDTA still bound to the protein can affect the protein's binding affinity for other metal ions. If metal and/or EDTA is still bound to the protein, one would not see a 2:1 ratio of metal to protein for DFsc or a 1:1 metal to protein ratio for UFsc. Determining the concentration of metal in our stock solutions is important so that we can be sure we are utilizing the correct amount of metal stock solution to see a 2:1 or 1:1 metal to protein ratio throughout our experiments, and to ensure our buffers and proteins are not contaminated.

1.2. Results and Discussion

The DFsc/UFsc family of proteins in this project involved introducing various mutations into the DNA sequence that codes for DFsc protein. Site-directed mutagenesis was performed using Phusion High-Fidelity DNA Polymerase and customized primers. The PCR was run under 3 separate conditions for each protein mutation so that we could find the optimal conditions for cloning and mutagenesis. The PCR reaction was loaded onto a 0.8% agarose gel and gel electrophoresis was performed to ensure mutagenesis was successful and that we amplified the desired sequence. I participated in introducing the E44L mutation and the Y18F mutation into UFsc wildtype. The gel shown below in figure 3, shows the presence of UFsc Y18F (lanes 1-3) but does not show the presence of UFsc E44L (lanes 4-6). Introducing Y18F into UFsc

wildtype was successful, and our group proceeded with expressing UFsc Y18F by transforming the plasmid into *E.coli* BL21(DE3). Since the mutagenesis of UFsc with E44L was not successful, it was decided to try Y18F first and to introduce E44L into UFsc E44Q.

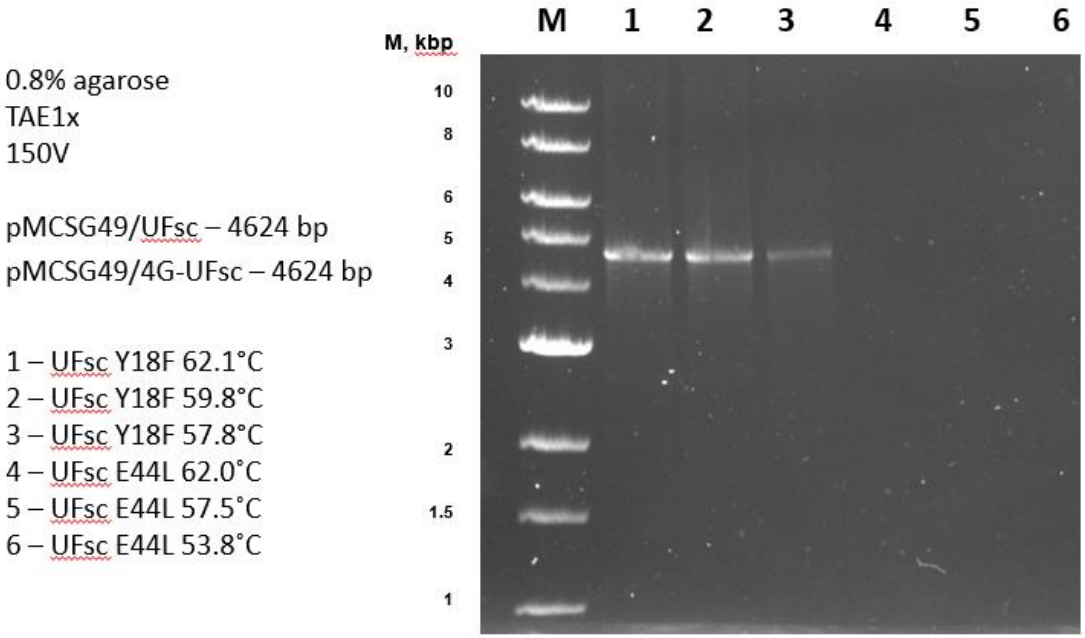

Figure 3. 0.8% Agarose DNA gel showing the presence of UFsc Y18F at 4624 bp (1-3) but not the presence of UFsc E44L (3-6).

Following successful mutagenesis, the plasmids containing the gene of interest were transformed into *E.coli* BL21 (DE3) and grown on an agar plate with ampicillin. A colony from our agar plate was used and grown in LB and the culture was induced with IPTG. The culture was pelleted via centrifugation, suspended in lysis buffer, and lysed by sonication. Soluble protein fraction was separated via centrifugation and filtered before being applied to Ni-NTA resin. The protein was eluted with elution buffer and the fractions containing protein were

exchanged into TEV cleavage buffer using a desalting column. Shown below is the purification of DFsc before TEV cleavage that I performed. The gel shows that the purification of DFsc prior to TEV cleavage was successful and the next step in the purification process can occur.

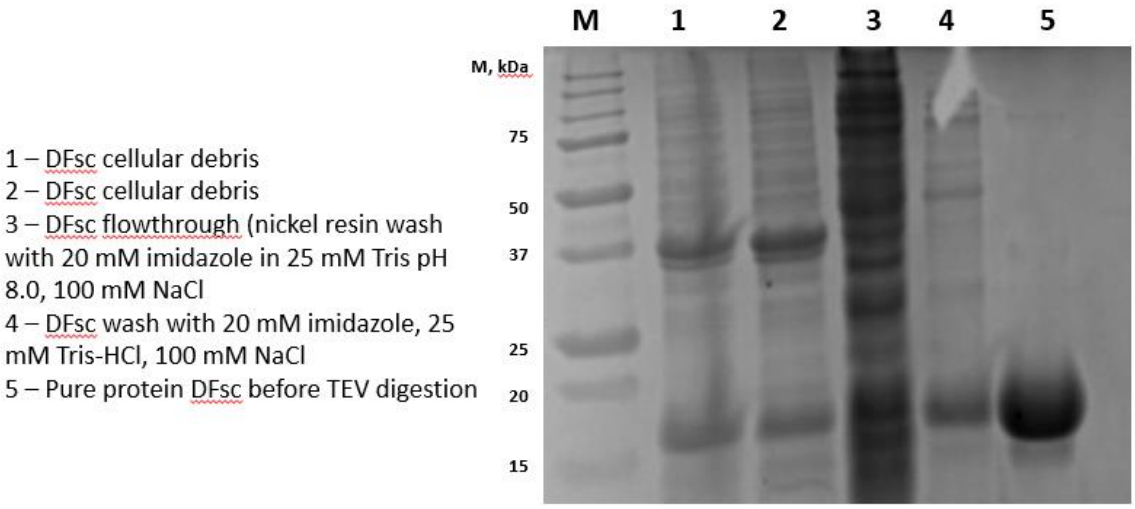

Figure 4: SDS-Page gel of DFsc protein expression in E. coli BL21(DE3). Lane M is the ladder. Lane 1 and 2 are cellular debris. Lane 3 is the DFsc Ni-NTA column flow through. Lane 4 is the wash sample and Lane 5 is the pure DFsc protein with His_6 tag before TEV digestion. The expected protein size is ~16.0 kDa.

The next step was to cleave the affinity tag (His_6 tag) with TEV protease in the presence of DTT. After TEV protease was added at a final ratio of 20/1 (protein/TEV), the solution was filtrated and incubated overnight (14-16 hours). Following digest, DTT and EDTA were removed via a desalting column and pure digested protein in storage buffer was applied to a Ni-NTA column and flow through fractions were collected. The purity of the sample fractions was checked via SDS-PAGE. Below is a gel of DFsc following TEV digestion that I performed. Looking at Lane 2, it can be concluded that TEV digestion successfully removed the His_6 affinity tag.

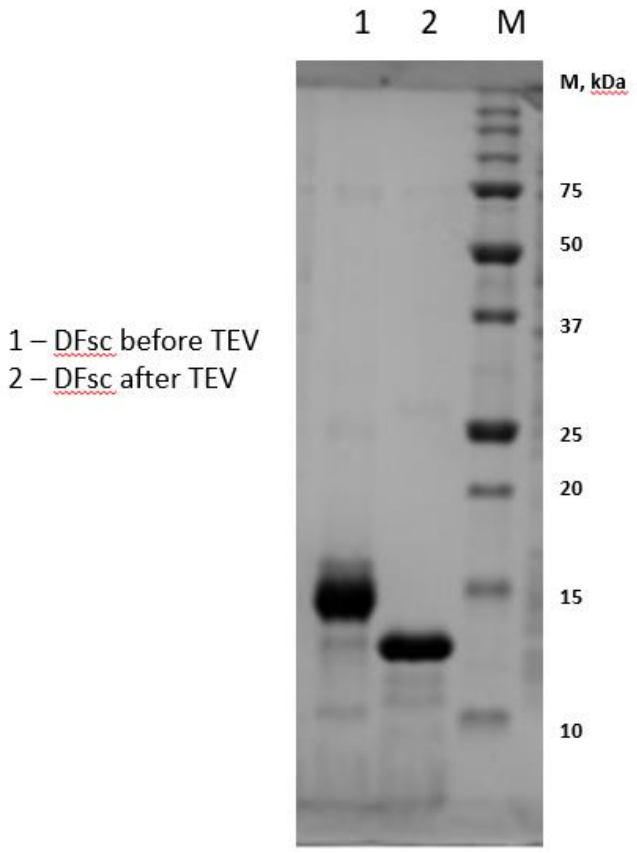

Figure 5. SDS-PAGE gel of DFsc protein following TEV digestion. Lane 1 is the sample before TEV digestion and Lane 2 is the DFsc protein following TEV cleavage. The expected protein size of non-cleaved His_6-tag DFsc is 16.0 kDa. The expected protein size of native DFsc following TEV digest is 13.49 kDa.This gel shows the successful removal of the affinity tag via TEV protease.

Following purification of the protein and removal of the affinity tag, the next step was to conduct experiments to ensure all EDTA was removed from the protein and to determine the binding stoichiometry of our proteins before running any kinetic experiments. We want to ensure that all DFsc proteins bind two metals and that UFsc and 4G-UFsc proteins bind only one.

EDTA is a metal chelator, meaning it acts as a binding agent to remove metals from solution[9]. If EDTA is present in our proteins during experimentation, it can affect the protein's binding affinity for other metal ions. Cobalt titration was employed in this process to ensure elimination of EDTA and to assess the stoichiometric ratio of Co(II) to protein. Cobalt was the metal of choice because cobalt is spectroscopically observable at low absorbance values[10]. By creating samples with different known concentrations of metal and measuring the absorbance of the samples, we were able to look at the protein's affinity for cobalt by constructing a titration curve from absorbance data. The curve should show an increase in absorbance up until the protein has been saturated with Co(II). Once saturation has occurred, there should be no increase in absorbance because the protein can no longer bind Co(II). A sharp inflection in the graph of the titration curve represents the stoichiometry of metal to protein for the given protein.

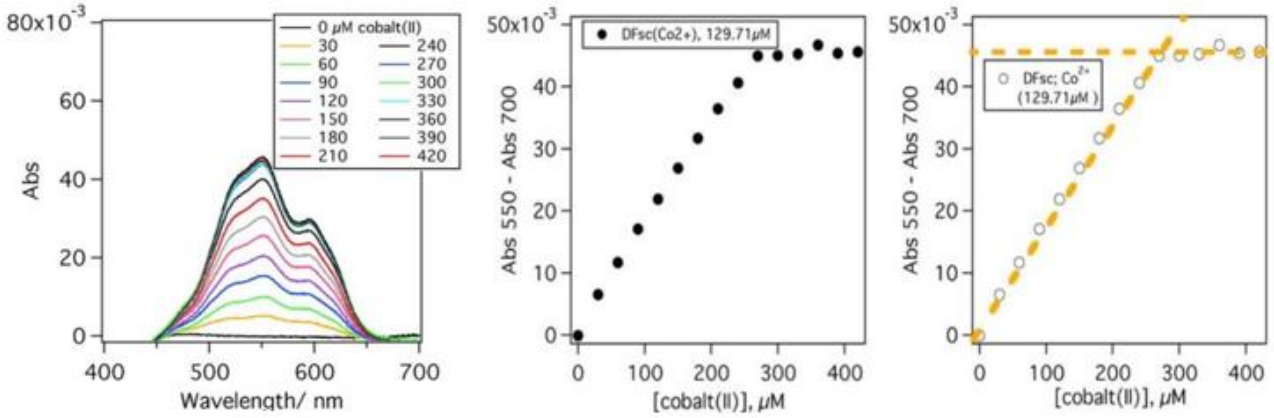

Figure 6. Cobalt Titration of DFsc. Titration curve shows successful elimination of EDTA and a DFsc:cobalt binding stoichiometry of 1:2.08.

Figure 6 shows a successful cobalt titration with DFsc that was performed by Jennifer Yoon, one of the graduate students I was collaborating with on this project. The titration curve is represented by a line that increases and then levels off once the protein has reached its saturation point. The linearity of the line that represents Co(II) binding prior to saturation shows that there was no substance interfering with the protein's binding affinity for Co(II) and is evidence that EDTA was successfully removed during the purification process. A sharp inflection in the graph occurs at the Co(II) concentration of 270 µM and 129.71 µM of protein, giving a DFsc:cobalt binding stoichiometry of 1:2.08. This sample of protein exhibits proper binding stoichiometry and can be used for experimentation.

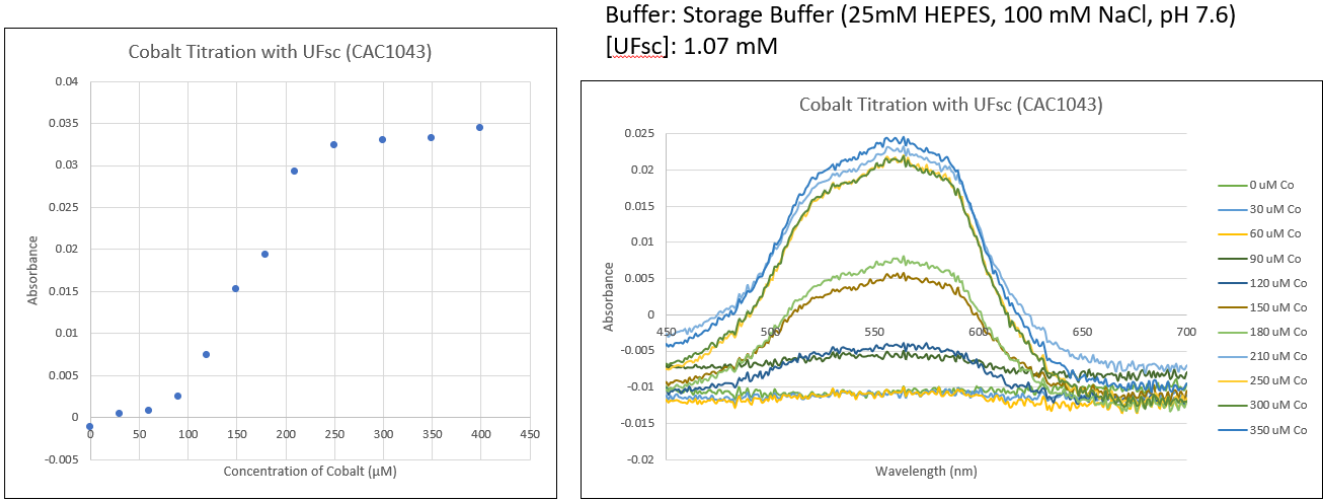

Figure 7: Cobalt titration of UFsc. Lack of linearity in UFsc's binding affinity for Co(II) prior to reaching saturation is evidence that EDTA is present. Protein needs to go through ultrafiltration to remove remaining EDTA.

Figure 7 shows a cobalt titration with UFsc that I performed. The portion of the graph that represents the binding of Co(II) to UFsc prior to saturation does not exhibit linearity as the titration graph in Figure 6 does. This lack of linearity in the titration graph means that

something is interfering with the protein's binding affinity for Co(II). We concluded that EDTA is still present in the UFsc protein sample and that the protein needs to go through additional purification protocol to eliminate the remaining EDTA before being utilized in experimentation.

Isothermal titration calorimetry was another method we employed to assess binding stoichiometry of our proteins. ITC allows us to monitor thermodynamic parameters of the metal binding to protein. The data gathered from ITC was fitted to the one set of sites model for UFsc and 4G-UFsc and two sets of sites model for DFsc by the software provided by the manufacturer to determine the stoichiometry. Panel A of Figure 8 shows the thermogram and integrated binding isotherm of DFsc-zinc binding. The integrated binding isotherm shows that DFsc has a DFsc:zinc binding stoichiometry of ~ 1:2. The integrated binding isotherm of UFsc-zinc binding shown in Panel B of Figure 8 shows that UFsc has a UFsc:zinc binding stoichiometry of ~ 1:1. A 4G-UFsc-zinc binding stoichiometry of ~1:1 is shown in the integrated binding isotherm of 4G-UFsc-zinc binding in Panel C of Figure 8. The proteins exhibit proper binding stoichiometry, with DFsc having a 2:1 ratio of metal to protein and UFsc and 4G-UFsc exhibiting a 1:1 ratio of metal to protein, and can therefore be used for experimentation.

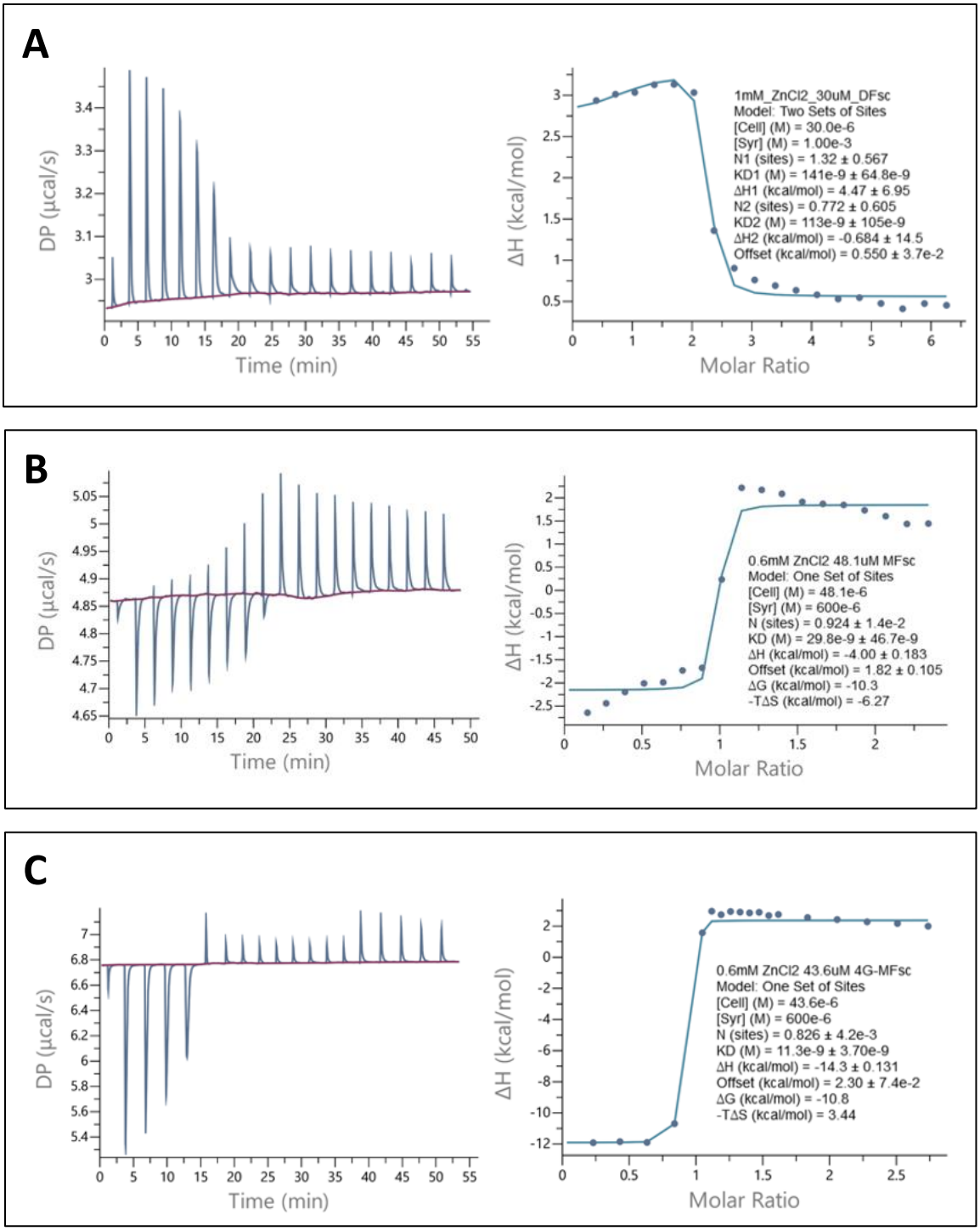

Figure 8. ITC analysis of zinc binding to DFsc, UFsc, and 4G-UFsc. (A) The thermogram and integrated binding isotherm of DFsc-zinc binding. DFsc exhibits a ~2:1 metal to protein binding stoichiometry with zinc. (B) The thermogram and integrated binding isotherm of UFsc-zinc binding. UFsc exhibits a ~1:1 metal to protein binding with zinc. (C) Based on the integrated isotherm of 4G-UFsc-zinc binding, UFsc exhibits ~1:1 metal to protein binding with zinc.

ICP analysis was utilized to detect for the presence of metal in our apo protein samples, and our buffer stock solutions. ICP analysis was also used to measure the concentration of our metal stocks to ensure we are as accurate as possible when utilizing these stocks in our experiments. Several preparation samples of apo DF proteins (DFsc, UFsc, 4G-UFsc, and mutants) were analyzed for metal content. The highest concentrations found were 0.08% Fe, 0.15% Co, 0.23% Mn, 0.56% cu, 1.60% Ni, and 3.2% Zn (fraction of protein bound to metal).

1.3. Conclusions and Future Work

DF family of proteins have been successfully expressed in *E.coli* BL21 (DE3) and purified. Via cleavage with TEV protease, the His_6 affinity tag was removed from proteins. EDTA was removed using ultrafiltration. Cobalt titration was utilized to verify the elimination of EDTA. ITC was employed to determine binding stoichiometry and apo protein samples were tested for presence of metal. Proteins are now ready to be used in experiments such as the catechol oxidation experiment described in the second chapter of this thesis.

1.4. Experimental

Cloning and mutagenesis. The cloning sequence that codes for DFsc protein was synthesized by BioBasic. The gene was cloned into pMCSG49 expression vector via ligase independent cloning. The sequence resulting from cloning has a N-terminal His_6-tag and a tobacco etch virus (TEV) protease recognition site. Site-directed mutagenesis was performed following standard protocols and utilizing Phusion High-Fidelity DNA Polymerase (ThermoScientific) and customized primers (Integrated DNA Technologies).

Expression of DFsc/UFsc. Plasmid containing the gene of interest was transformed into *E.coli* BL21 (DE3) (New England Biolabs) and the cells were grown on agar/LB plates with Ampicillin (Amp) (100 µg/mL) overnight at 37˚C. The next day, the starter culture grown from a single colony was inoculated in LB (Luria Bertani) medium supplemented with 100 µg/mL Amp and incubated overnight at 37˚C with vigorous shaking. The following day, 10 mL of the overnight culture were diluted 1:100 in LB medium supplemented with Amp and this culture was incubated at 37˚C with vigorous shaking until OD_{600} reached 0.6 – 0.7. The culture was induced with IPTG to a final concentration of 0.5 mM and continued to grow at 30˚C. After 4 hours of expression, the culture was pelleted by centrifugation at 4˚C (20 min, 4,000 g). The pellets were analyzed by SDS-PAGE for protein expression.

Purification of DFsc/UFsc. The cell pellet was resuspended in lysis buffer (5mL for 1 g of cell paste) containing 25 mM Tris-HCl, 20 mM imidazole, 100 mM NaCl (pH 8) with 0.5 mM PMSF (phenylmethylsulfonyl fluoride; protease inhibitor). The cells were lysed by sonication on ice with 20 second pulses for ten minutes. The lysate was centrifuged at 20,0000 g for 30 minutes at 4˚C to remove cell debris. The supernatant was filtered through 0.22 µm pore size PES filter (UltraCruz) before being applied onto a Ni-NTA column (Clontech, 2 mL). The column was washed with 50 mL lysis buffer and the protein was eluted with buffer containing 25mM Tris-HCl, 250 mM imidazole, 100 mM NaCl (pH 8). Fractions containing protein were exchanged into TEV cleavage buffer (50 mM Tris HCl, 75 mM NaCl, pH 8) using a desalting column (BioRad, Econo-Pac 10 DG). The affinity tag was cleaved with TEV protease in the presence of 1 mM DTT and 2 nM EDTA. The TEV protease was added to a final (A_{280} protein)/(A_{280} TEV protease) ratio of 20/1. This solution was then sterilized by filtration through a 0.22 µm PES filter and

incubated at 34˚C overnight. Following TEV digest, DTT and EDTA were removed on a desalting column and the pure digested protein in storage buffer (25 mM HEPES, 100 mM NaCl, pH 7.6) was collected in the flow through fractions from the Ni-NTA column. The purity of the final samples was confirmed by SDS-PAGE analysis. Protein concentration was determined via UV-Vis spectroscopy by measuring A_{280} using the calculated extinction coefficient of 8,480 $M^{-1}cm^{-1}$.

Protocol to remove any bound protein. The protein samples were treated with 5 equivalents of EDTA, incubated for 30 minutes at room temperature to chelate any metal, and then passed though a desalting column to remove EDTA. An ultrafiltration step was performed to eliminate residual EDTA. The protein was applied to a centrifugal filter with a 10 kDa molecular weight cut off (MWCO) (Corning Spin-X UF), diluted with EDTA free buffer (25 mM HEPES, 100 mM NaCl, pH 7.6), and centrifuged at 4˚C for 15 min at 3,000 g to concentrate protein. This concentration/dilution procedure was repeated 3 times. The concentrated protein solution of about 2-3 mL was dialyzed against 25 mM HEPES, 100 mM NaCl (pH 7.6) for 2 hours at 4˚C using Slide-A-Lyzer G2 dialysis cassettes (ThermoFisher Scientific) with a MWCO of 7 kDa. Dialysis was repeated 2 times and was followed by overnight incubation at 4˚C.

Cobalt Titration. Cobalt titration was employed in this process to verify the elimination of EDTA. The stoichiometric ratio of Co(II) to protein was determined by titration of DF proteins with 0 µm to 420 µM $CoCl_2$. 150 µM protein in 25 mM HEPES, 100 mM NaCl (pH 7.6) was incubated with cobalt salt ($CoCl_2$) overnight. The following day, the samples were centrifuged at 15,000 rpm for 15 min to pellet any precipitate. UV-Vis spectra of mixtures were obtained from 400-700 nm using Agilent Cary 60 UV-Vis spectrophotometer. Λ_{max} was plotted for each Co(II)-protein complex as a function of added Co(II).

ICP Analysis. All proteins were evaluated by ICP-OES for the presence of metal. Protein stock solutions were diluted using storage buffer (25 mM HEPES, 100 mM NaCl, pH 7.6) containing 2% HNO_3 to a final concentration of 25 μM in 3 mL. The concentration of Zn, Mn, Fe, Co, Ni, and Cu were measured using ICP-OES (Perkin Elmer Optima 3300 DV) in order to determine elemental concentration. Following this, several preparations of apo DF proteins were analyzed for metal content.

Isothermal titration calorimetry (ITC). For the purposes of the purification part of this experiment, ITC was utilized to assess the stoichiometric ratio of metal to protein. The stoichiometric rations of metal binding to DFsc, UFsc, and 4G-UFsc were monitored using a MicroCal PEAQ-ITC instrument (Malvern). The exact concentration of protein was determined via UV-Vis spectroscopy. Stock solutions of metal salts (50 mM) were prepared in water and diluted to the appropriate concentrations in buffer (25 mM HEPES, 100 mM NaCl, pH 7.6). The concentrations of these metal stock solutions were confirmed by ICP-OES. The protein that was placed in the calorimeter cell was titrated with metal solutions by automatic injections at 25˚C with 750 rpm stir speed. Microcal PEAQ-ITC Analysis software, provided by the manufacturer, was used to perform baseline correction and integration of the peaks corresponding to each injection. The data was fitted to the one set of sites model for UFsc and 4G-UFsc, and the two sets of site model was used for DFsc to determine the stoichiometry (n).

Chapter 2: Semiquinone Radical Stabilization

2.1. Introduction

A radical is defined as an unstable and generally highly reactive species. Some enzymes can successfully employ radicals in challenging chemical transformations to promote reactions that are necessary for life[1–3]. Ribonucleotide reductase (RNR) is an example of such an enzyme. RNR is a ubiquitous enzyme that catalyzes the conversion of ribonucleotides to deoxyribonucleotides, an essential step in DNA synthesis[11]. RNR requires metallofactors to initiate radical-based nucleotide reduction. This enzyme is a complex of two proteins. One complex contains an iron center and a tyrosine moiety sidechain that exists as a free radical stabilized by the iron center[11,12]. This radical has access to the substrate-binding pocket and is essential for enzyme activity[12]. The mechanism by which RNR, and other similar enzymes, stabilize thermodynamically and kinetically unstable species is poorly understood.

Recently, model systems have been used to study the mechanisms used by proteins to stabilize radicals. The DeGrado lab has shown that a zinc-containing protein derived from DFsc [3His-GZDFsc-Zn_2] stabilizes a semiquinone radical anion which is formed by comproportionation of 3,5-di-tert-butylcatechol (DTBC) and the corresponding quinone[2]. This scheme is shown in the figure below. DTBC is often employed in laboratory studies as a model substrate for tracking the chemistry of catechol oxidation and has been used to establish basic principles that govern the mechanisms of radical enzymes[3]. Based on the research published by the DeGrado lab, our lab wanted to explore the role of metal in radical production in model

systems such as the DF family of proteins. Exploring the role of metals may give insight into the factors that contribute to radical stabilization by proteins.

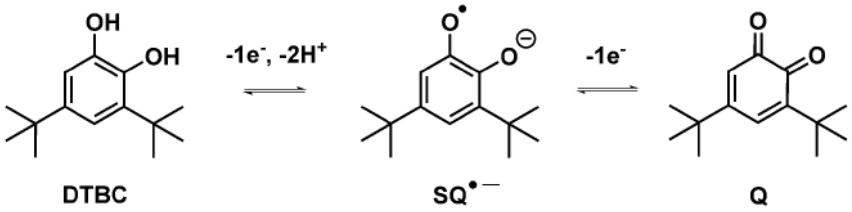

Figure 9. Catechol oxidation scheme. The semiquinone radical anion ($SQ^{\bullet -}$) is an unstable intermediate between the fully reduced catechol (DTBC) and the fully oxidized quinone (Q) states[2,3].

The Makhlynets lab discovered that oxidation of DTBC by dioxygen in the presence of zinc-bound DFsc produces semiquinone radical anion with a yield comparable to the DFsc-derived protein used by the DeGrado lab[3]. Knowing this, our lab utilized DFsc as a model protein to understand the role of metal in radical stabilization. We tested DFsc in its apo form and DFsc bound with one metal ion. The results showed that apo DFsc promoted no radical production and that DFsc in the presence of one equivalent of zinc promoted formation of the semiquinone radical anion with approximately 30% less yield compared to fully metallated protein[3].

Further analysis was conducted to evaluate metals contribution to radical stabilization. By mutating Glu104 in DFsc to histidine DFsc was converted into a single metal-binding protein (UFsc). The channel that leads to the metal center in UFsc was widened by introducing A10G, A14G, A43G, and A47G, leading to the creation of 4G-UFsc. The Makhlynets lab found that both promote semiquinone radical formation in the presence of one equivalent of Zn^{2+}. The radical yield with 4G-UFsc with one equivalent of zinc was comparable as the radical yield for DFsc with

two equivalents of zinc bound[3]. This demonstrated that only one metal ion is needed to fulfill the radical stabilization role in the DF family of designed proteins. The next step in this study was to measure $SQ^{\bullet -}$ formation for DFsc, UFsc, and 4G-UFsc in the presence of 1 or 2 equivalents of various metal ions (Ni^{2+}, Co^{2+}, Mn^{2+}, and Zn^{2+}) to determine whether the identity of the metal ion and the number of metal ions influenced protein's ability to participate in radical stabilization.

2.2. Results and Discussion

My work on the semiquinone radical stabilization part of this project was to run catechol oxidation experiments in hopes to replicate the data produced by Jennifer Yoon and Dr. Areetha D'Souza. The experiments that I conducted involved working with DFsc in the presence of 1 or 2 equivalents of various metals. My first attempt at running the experiment was unsuccessful because there was precipitate that formed in my DFsc-metal solutions following the addition of DTBC and oxygenated buffer. The precipitate disrupted the UV-Vis readings and changes were made to the protocol to adjust for this. For my second attempt at the catechol oxidation experiment with DFsc in the presence of 1 or 2 equivalents of various metals the results produced were similar to those of Jennifer and Dr. D'Souza. To adjust to the formation of a precipitate in samples, the solutions were spun down using an Eppendorf centrifuge prior to collection of UV-Vis spectrum.

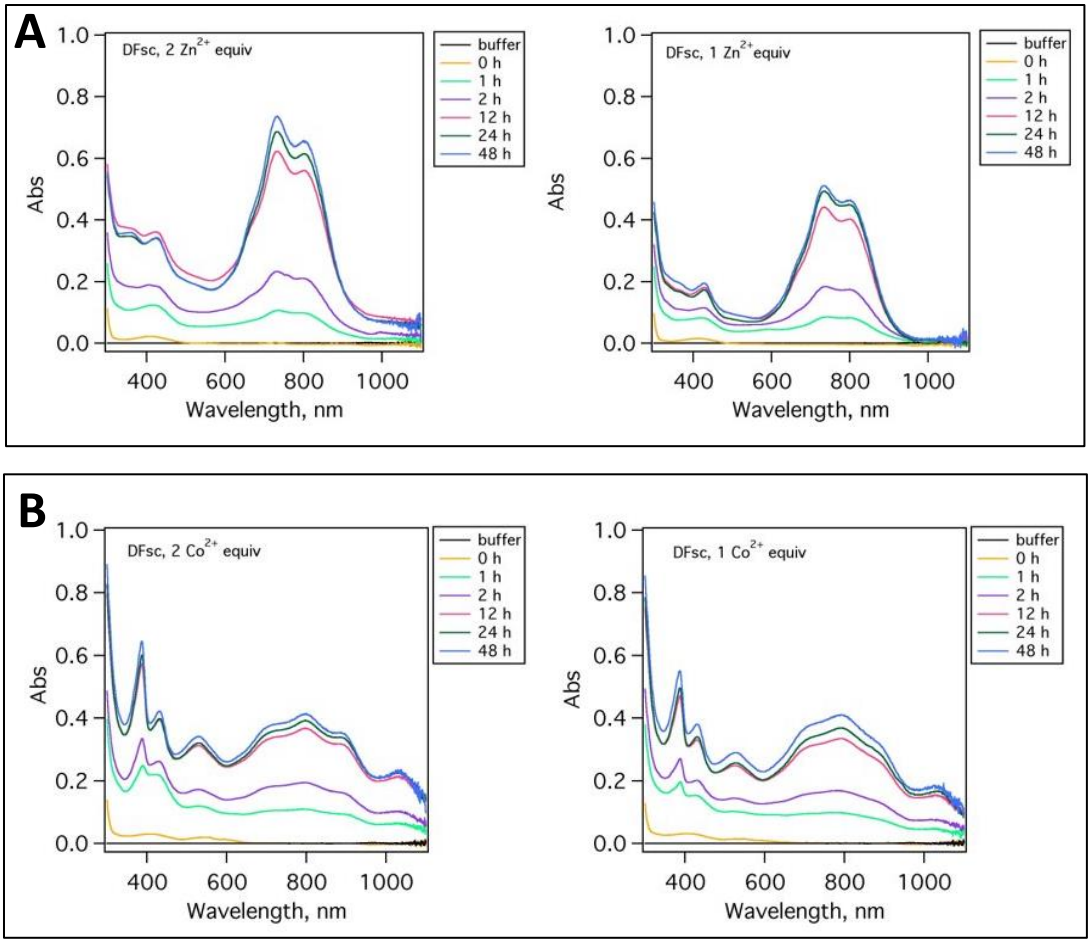

Figure 10. DTBC oxidation by dioxygen in presence of DFsc and two equivalents of metal. (A) UV-Vis spectra of reaction mixtures containing DFsc with one equivalent and two equivalents of zinc (B) UV-Vis spectra of reaction mixtures containing DFsc with one equivalent and two equivalents of cobalt. Spectra of samples were taken immediately after addition of oxygenated buffer and after 1, 2, 12, 24, and 48 hours.

Semiquinone is unstable as a free radical. Binding to DFsc stabilizes the $SQ^{\bullet}$ and the presence of the [DFsc-$Zn(II)_2$]-$SQ^{\bullet}$ moiety is detected via UV-Vis spectroscopy as a broad banned spanned 750-850 nm^2. The semiquinone radical appears as a colored species with λ_{max} ~760 nm. DTBC is seen at around 400 nm in UV-Vis spectra. As shown by a broad band spanned 740-850 nm in Figure 10A, DFsc promotes semiquinone radical formation and stabilizes the semiquinone radical in the presence of one equivalent of Zn^{2+}. The radical yield slightly

increases for DFsc with 2 equivalents of zinc bound which is represented in figure 10A by an increase of absorbance at around 760 nm. DFsc promotes semiquinone radical formation in the presence of one equivalent of Co^{2+} (Figure 10B), but not to the extent as seen with Zn^{2+}. Addition of the second Co^{2+} ion does not seem to lead to an increase in the yield of the radical as no significant increase in the absorption around 760 nm is observed following the addition of the second metal ion (Figure 10B).

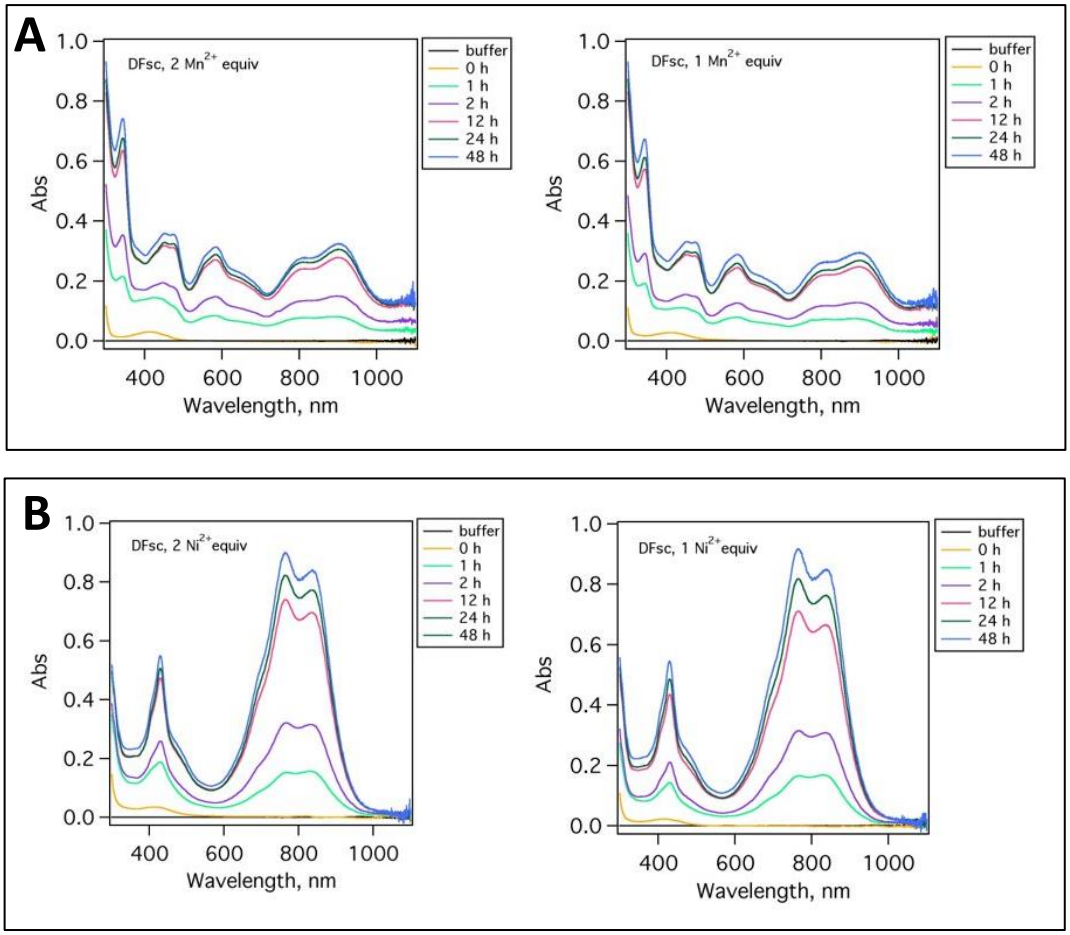

Figure 11. DTBC oxidation by dioxygen in presence of DFsc and two equivalents of metal. (A) UV-Vis spectra of reaction mixtures containing DFsc with one equivalent and two equivalents of manganese (B) UV-Vis spectra of reaction mixtures containing DFsc with one equivalent and two equivalents of nickel. Spectra of samples were taken immediately after addition of oxygenated buffer and after 1, 2, 12, 24, and 48 hours.

Formation of the semiquinone radical was formed by DFsc in the presence of one equivalent of Mn^{2+}, shown in figure 11A by absorption at ~760 nm. The broad band of absorption at 740-850 nm signifies presence of [DFsc-$Mn(II)_2$]-$SQ^{\bullet}$ moiety, meaning DFsc in the presence of one equivalent of Mn^{2+} stabilizes the semiquinone radical. Since no increase in the absorption at 760 nm is seen after the addition of a second Mn^{2+} ion, the second metal ion does not increase the yield of the radical (Figure 11A). The absorption at 760 nm for DFsc in the presence of Mn^{2+} is lower than DFsc in the presence of the other metals (Figure 10), meaning $SQ^{\bullet-}$ formation in the presence of Mn^{2+} is low. DFsc bound to one equivalent of Ni^{2+} shows the highest stabilization represented in UV-Vis spectra as having the highest absorbance at 760 nm. Since there was no significant increase in the absorption at 760 nm following the addition of a second Ni^{2+} ion (Figure 11B), addition of the second equivalent of Ni had no effect on radical production.

2.3. Conclusions and Future Work

DFsc, UFsc, and 4G-UFsc are able to stabilize a semiquinone radical by binding the radical and keeping the radical tightly bound within the protein's binding pocket. We found that radical stabilization is not dependent on the number of metal ions bound to the protein. Addition of one equivalent of the metal results in radical stabilization and addition of the second metal ion only leads to minor increase in the yield of the radical, or in some cases no increase is observed. Based on semiquinone radical experiments run with various metals, we discovered that the yield of the radical is dependent on the nature of the metal ion. DFsc bound to nickel showed the highest stabilization, making it the best metal for optimal radical stabilization.

Future work with semiquinone radical stabilization will include EPR analysis which is a magnetic spectroscopy method that can be utilized to further confirm the semiquinone radical binding to DFsc. Redox titration experiments will be conducted to quantitatively characterize the degree of stabilization of the semiquinone radical anion.

2.4. Experimental

UV-Vis assay for catechol oxidation. The kinetics measurements of the catechol oxidation experiment were performed on Agilent Cary 60 UV-Vis spectrophotometer using a 1 mL quartz cuvette with a 1 cm path length. A solution of 3,5-di-tert-butyl catechol (DTBC) was freshly prepared in methanol at 20 mM concentration. An appropriate amount of DTBC solution was added to protein in non-oxygenated buffer containing 25 mM HEPES, 100 mM NaCl, pH 7.6 (500 µL total volume). Pure dioxygen gas was bubbled for 30 min through buffer solution kept on ice to prepare oxygen-saturated buffer (25 mM HEPES, 100 mM NaCl, pH 7.6). 500 µL of oxygenated buffer was added to the DTBC-protein mixture and UV-Vis spectrum was collected immediately after 0, 1, 2, 12, 24,and 48 hours of incubation at room temperature. The final concentrations of reagents within the mixture samples were as follows: 50 µM protein, 500 µM substrate in 25 mM HEPES, 100 mM NaCl (pH 7.6) and ~ 0.65 mM O_2. An appropriate amount of metal from 10 mM stock in water was added to protein to achieve one equivalent of metal for UFsc and 4G-UFsc, and two equivalents of metal for DFsc. Protein in buffer with metal mixtures were incubated at room temperature for 15 minutes prior to addition of substrate and oxygenated buffer.

Chapter 3: Establishing Coordination Geometry for DF Family of Proteins

3.1. Introduction

DFsc binds two metals and the coordination environment of the two metal-binding sites within this protein is symmetric[6,7]. Since UFsc and 4G-UFsc bind only one metal ion, the symmetry that is seen within the coordination environment of DFsc is not present in the UF proteins. Our group wanted to establish coordination geometry of the metal binding site of UFsc and 4G-UFsc. To do so, we introduced mutations to the binding pocket (Table 1) and utilized ITC and CD analysis to determine how introducing mutations to the binding pocket affects the protein's confirmation, stability, and binding affinity for metal ions. The goal of this research is to address the question of which ligands are important for metal binding.

Our lab has previously shown that iron binds to the E44 site within the binding pocket of the DF family of proteins[3]. We set up experiments to test protein binding with various metal ions (manganese, zinc, cobalt, and nickel) in hopes to establish coordination geometry. The questions we hope to find answers to are whether metals occupy the same coordination environment or whether metals have preference to another type of ligand arrangement.

3.2. Results and Discussion

My work on this part of the DFsc/UFsc project involved collaborating with graduate student, Alona Kulesha. Alona had already produced CD data of UFsc mutants and 4G-UFsc mutants in the absence and presence of zinc. The task given to me was to focus on E44 mutants (Table 2) and to run CD analysis on these mutants to determine whether her data was reproducible. Utilizing CD analysis was a way for us to determine the secondary structure and

folding properties of our proteins and to determine how mutations affect confirmation, stability, and interactions of the protein.

Table 2: UFsc and 4G-UFsc E44 mutants analyzed via CD.

UFsc and 4G-UFsc Mutants for CD Analysis
E44Q
E44L & Y18F (double mutant)

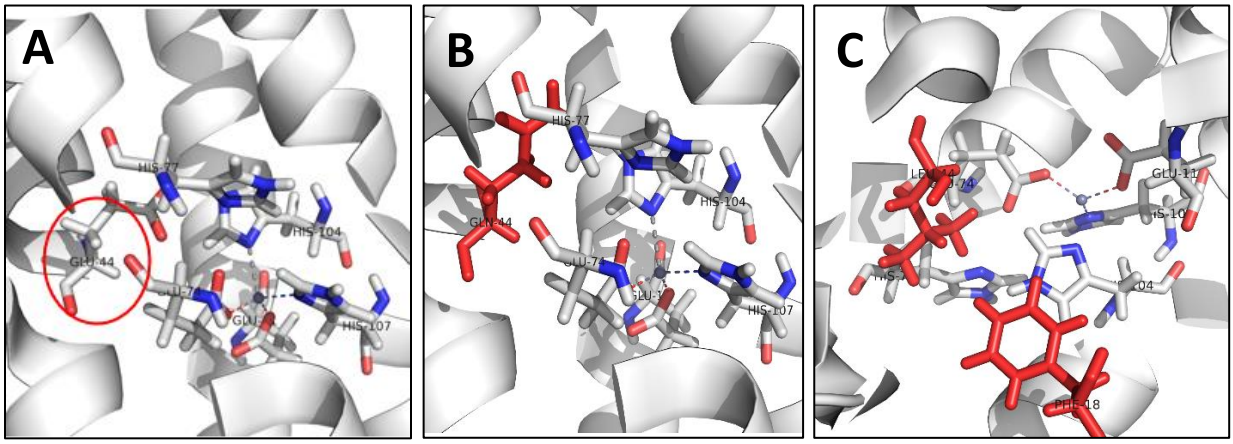

Figure 12. Mutagenesis of UFsc in PyMOL. (A) UFsc. The red circle highlights the residue at position 44 that our group introduces mutations at. (B) E44Q mutant. The glutamate at position 44 was mutated to a glutamine. (C) E44L Y18F mutant. Two mutations were introduced into UFsc at positions 44 and 18. At position 44, the glutamate was mutated to leucine and at position 18, the tyrosine was mutated to phenylalanine.

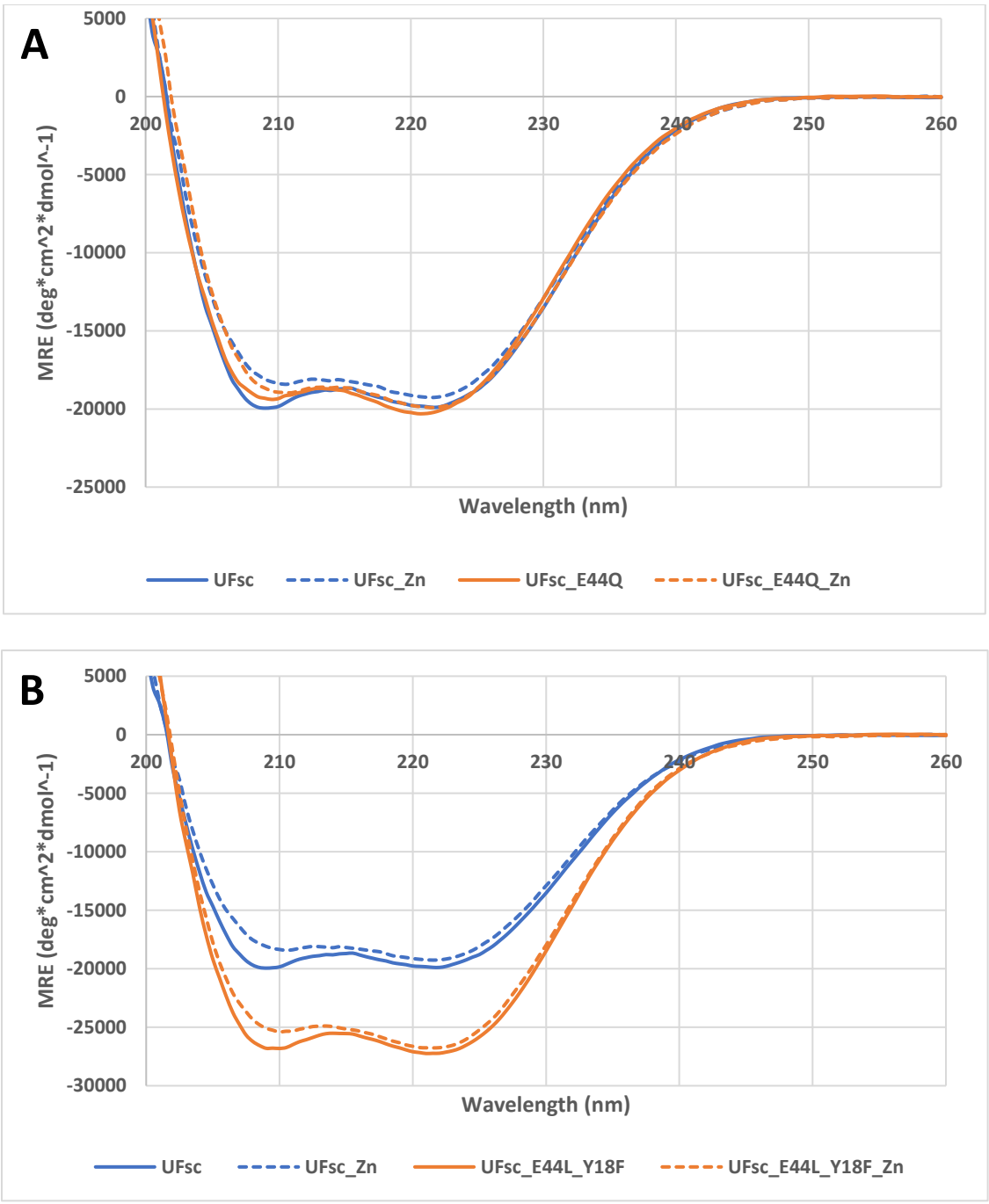

Figure 13. CD analysis of introduction of mutations at position 44 in UFsc (A) E44Q (B) E44L Y18F. For the graphs, the solid line represents protein with no metal bound while the dashed lines represent protein bound with zinc. The blue lines indicate the wild type protein and the orange lines represent the mutants.

Introducing the E44L Y18F mutation significantly changed the degree of protein helicity. This is seen in Figure 13B as the difference between the solid blue (UFsc) and solid orange (4G-UFsc E44L Y18F) lines and this difference indicates that introducing the E44L Y18F mutation changed the secondary structure and folding properties of the UFsc. By examining the differences in the UFsc-Zn (blue dashed) and the UFsc E44L Y18F-Zn (orange dashed) lines, it can be concluded that the mutation affected the protein's interaction with zinc. Introducing the E44Q mutation slightly changed the secondary structure and folding properties of UFsc (Figure 13A), but not to the extent of the E44L Y18 F mutation. The data from the CD analysis that I conducted was compared to Alona's data and the following conclusion was drawn. Introduction of all mutations at position 44 of UFsc led to the increase in the degree of protein helicity. The formation of a coiled coil structure was suggested for all proteins due to the ratio of $\theta_{222\ nm}/\theta_{208\ nm}$ being 1.0-1.1 for all proteins.

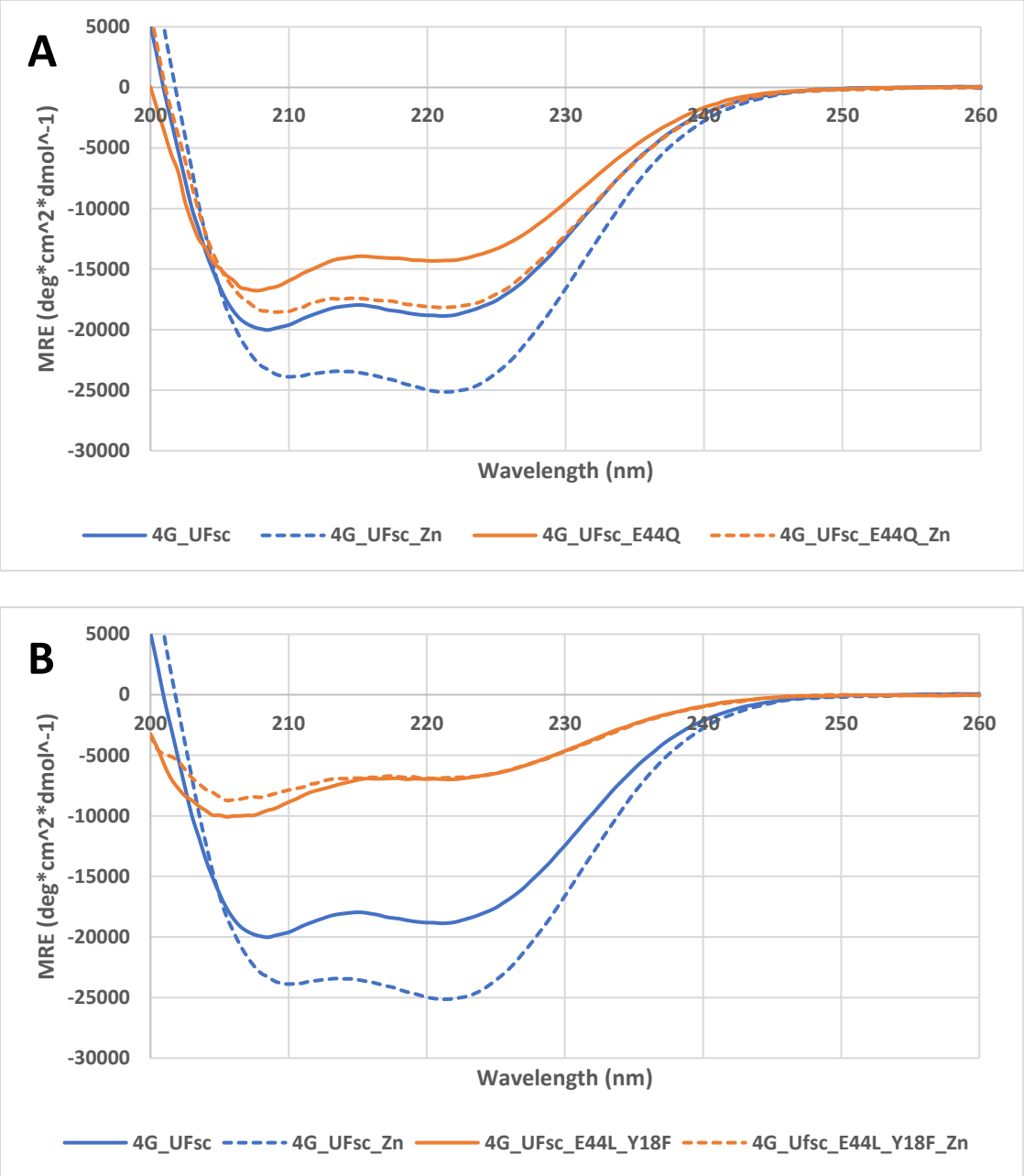

Figure 14. CD analysis of introduction of mutations at position 44 in 4G-UFsc (A) E44Q (B) E44L Y18F. For the graphs, the solid line represents protein with no metal bound while the dashed lines represent protein bound with zinc. The blue lines indicate the wild type protein and the orange lines represent the mutants.

As depicted in the graph in Figure 14A by the difference in the 4G-UFsc (solid blue) and 4G-UFsc E44Q (solid orange) lines, the introduction of the E44Q mutation changed the

secondary structure and folding properties of 4G-UFsc by significantly changing the degree of protein helicity. The variability in the 4G-UFsc-Zn (blue dashed) and 4G-UFsc E44Q-Zn (orange dashed) lines reflect how introduction of the E44Q mutation influenced the protein's interaction with zinc. The E44Q mutation did not influence protein structure and interaction with zinc to the extent that the E44L Y18F mutation did. The discrepancy between the 4G-UFsc (blue) and 4G-UFsc E44L Y18F (orange) lines shown in Figure 14B are much larger than the discrepancies seen with introduction of mutation E44Q (Figure 14A). Specifically, the discrepancy between the dashed blue (4G-UFsc-Zn) and dashed orange (4G-UFsc E44L Y18F-Zn) line in Figure 14B is significant, meaning the introduction of mutation E44L Y18F greatly influenced 4G-UFsc's interaction with zinc. Compilation of the CD data I produced with the data Alona produced led to the following conclusions. All mutations introduced at position 44 in 4G-UFsc led to the increase in the degree of protein helicity. The ratio of $\theta_{222\ nm}/\theta_{208\ nm}$ was 1.0-1.1 for all proteins, suggesting the formation of the coiled coil structure.

Referring to the work with ITC, I did not conduct my own experimentation and analysis but instead assisted Alona with ITC analysis of E44 mutants. We utilized ITC to observe changes in thermodynamic parameters of metal binding to E44 mutants. We not only wanted to test mutations to the binding pocket, we also sought out to test how changing the ligand influenced thermodynamic parameters such as stoichiometry, enthalpy of complex formation (ΔH), and equilibrium dissociation constant (K_d). The ligands we tested were nickel (II), cobalt (II), manganese (II), and zinc (II). Zinc binding to UFsc and 4G-UFsc were measured by competition titration with triethylenetetramine (TETA) complex.

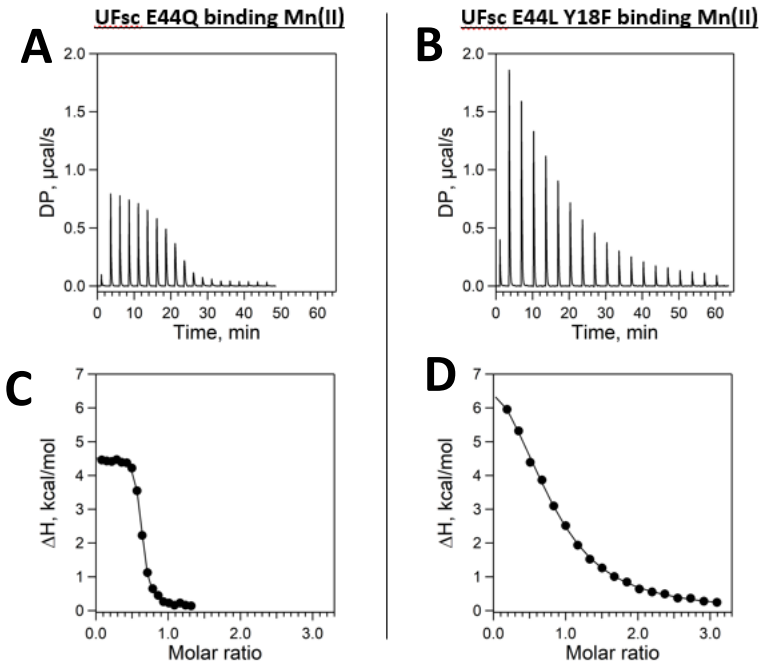

Figure 15: ITC analysis of UFsc E44 mutants binding to manganese. (A) Thermogram of UFsc E44Q binding Mn(II) (B) Thermogram of UFsc E44L Y18F binding Mn(II) (C) Integrated binding isotherm of UFsc E44Q binding to Mn(II) (D) Integrated binding isotherm of UFsc E44Q binding to Mn(II).

Table 3. ITC thermodynamic parameters for UFsc, UFsc E44Q, and UFsc E44L Y18F binding to Mn(II).

Metal	Parameters	UFsc	UFsc E44Q	UFsc E44L Y18F
Mn (II)	N	0.755	0.607	0.774
	Kd, nM	173	560	36600
	ΔH, kcal/mol	2.39	4.37	8.92

Figure 15 shows the thermograms and integrated binding isotherms of the UFsc E44Q and UFsc E44L Y18F analyses that I assisted with. Each ITC analysis was run 3 times. The averaged thermodynamic parameters are shown above in table 3. K_d, the equilibrium dissociation constant is the inverse of K_a, the equilibrium association constant. K_a and K_d relate to binding affinity. When K_a is high and K_d is low, the protein has a high affinity for the ligand. UFsc E44Q has a higher K_d value than UFsc which means that introduction of the E44Q mutation

decreased the protein's affinity for Mn(II). The K_d for the double mutant E44L Y18F is more than 200x greater than the K_d for wild type UFsc. The introduction of mutations E44L and Y18F drastically decreased the protein's affinity for Mn(II).

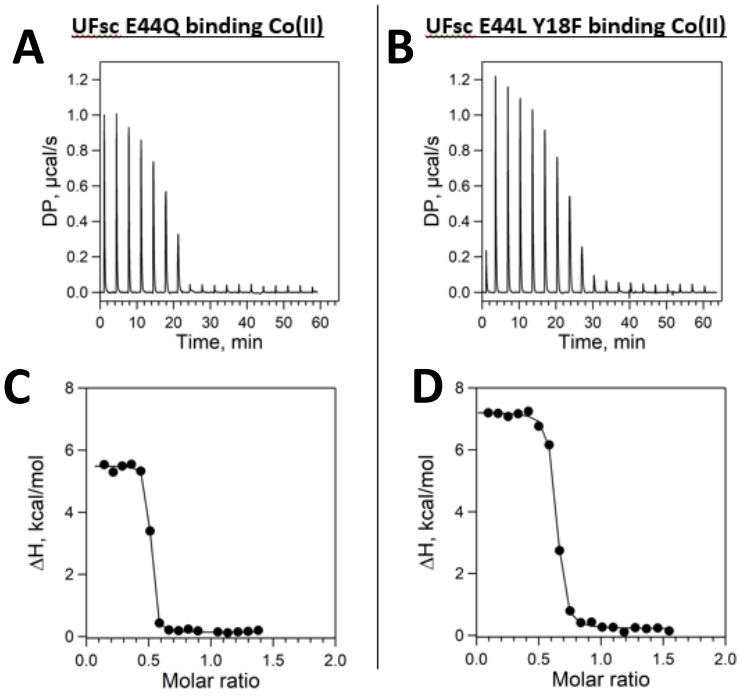

Figure 16: ITC analysis of UFsc E44 mutants binding to cobalt. (A) Thermogram of UFsc E44Q binding Co(II) (B) Thermogram of UFsc E44L Y18F binding Co(II) (C) Integrated binding isotherm of UFsc E44Q binding to Co(II) (D) Integrated binding isotherm of UFsc E44Q binding to Co(II).

Table 4. ITC thermodynamic parameters for UFsc, UFsc E44Q, and UFsc E44L Y18F binding to Co(II).

Metal	Parameters	UFsc	UFsc E44Q	UFsc E44L Y18F
Co (II)	N	0.617	0.485	0.606
	Kd, nM	269	51.7	172
	ΔH, kcal/mol	1.46	5.35	6.99

The average K_d values across the 3 trials are shown in Table 4. The K_d values of UFsc E44Q and UFsc E44L Y18F are smaller than the K_d value of wildtype UFsc. Since K_d is the inverse

of K_a, this means that the equilibrium association constants for UFsc E44Q with Co(II) and UFsc E44L Y18F with Co(II) is higher than that of native UFsc with Co(II). This means that introduction of mutations at position 44 in UFsc increased the protein's affinity for Co(II).

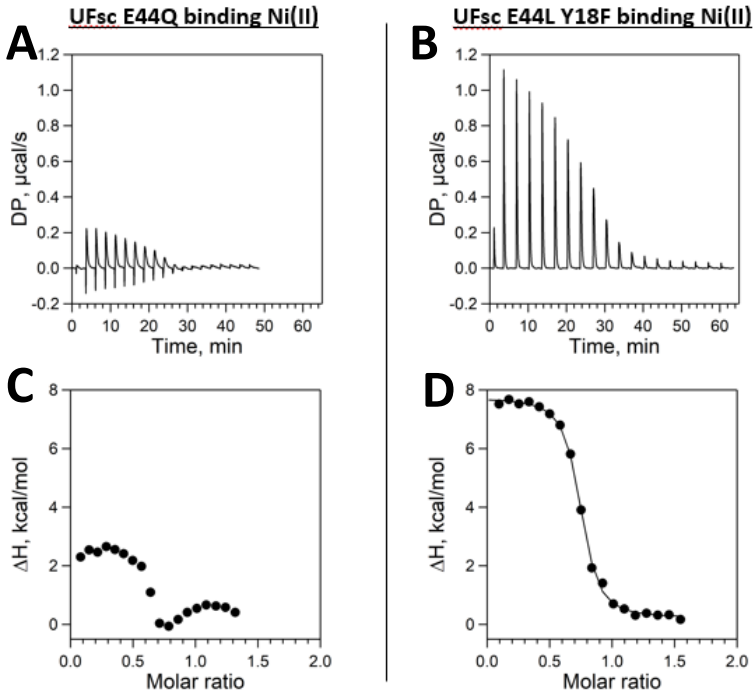

Figure 17: ITC analysis of UFsc E44 mutants binding to nickel. (A) Thermogram of UFsc E44Q binding Ni(II) (B) Thermogram of UFsc E44L Y18F binding Ni(II) (C) Integrated binding isotherm of UFsc E44Q binding to Ni(II) (D) Integrated binding isotherm of UFsc E44Q binding to Ni(II).

Table 5. ITC thermodynamic parameters for UFsc, UFsc E44Q, and UFsc E44L Y18F binding to Ni(II).

Metal	Parameters	UFsc	UFsc E44Q	UFsc E44L Y18F
Ni (II)	N	0.632	No binding	0.716
	Kd, nM	112		824
	ΔH, kcal/mol	4.12		7.5

As seen in the integrated binding isotherm of UFsc E44Q binding to Ni(II), no binding curve was established (Figure 17), meaning UFsc E44Q does not bind to nickel; however, wild type UFsc binds to Ni(II). Mutating the residue at position 44 to a leucine (E44L) and adding a

second mutation, Y18F, does bind Ni(II), but with a lower affinity, which can be seen by an increase in the dissociation constant for UFsc E44L Y18F compared to that of UFsc (Table 5). Based on this experiment it seems the identity of the residue at position 44 is important for UFsc to bind nickel.

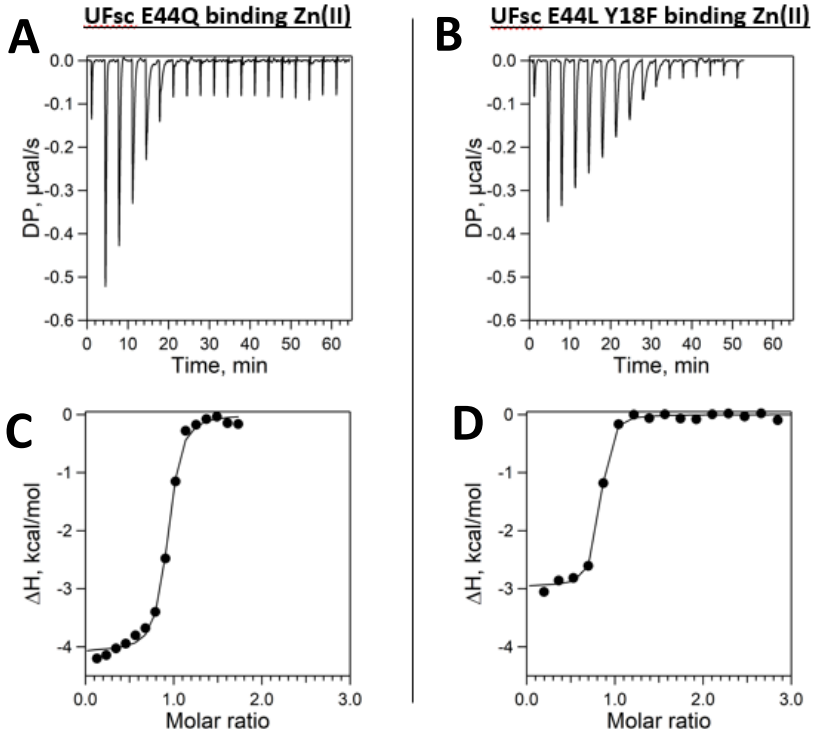

Figure 18: ITC analysis of UFsc E44 mutants binding to zinc obtained from the competition titration with TETA. (A) Thermogram of UFsc E44Q binding Zn(II) (B) Thermogram of UFsc E44L Y18F binding Zn(II) (C) Integrated binding isotherm of UFsc E44Q binding to Zn(II) (D) Integrated binding isotherm of UFsc E44Q binding to Zn(II).

Table 6. ITC thermodynamic parameters for UFsc, UFsc E44Q, and UFsc E44L Y18F binding to Zn(II).

Metal	Parameters	UFsc	UFsc E44Q	UFsc E44L Y18F
Zn (II) (competition with TETA)	N	0.993	0.889	0.760
	Kd, nM	0.0761	0.512	0.285
	ΔH, kcal/mol	-1.85	-0.53	0.603

Based on the integrated binding isotherms of UFsc E44Q and UFsc E44L Y18F (Figure 18C and Figure 18D), both mutants bind Zn(II). The K_d values of both mutants is higher than the wild type protein, meaning the K_a values of the mutants are lower than that of the wild type UFsc. Introduction of mutations at position 44 of UFsc decrease the protein's binding affinity for Zn(II).

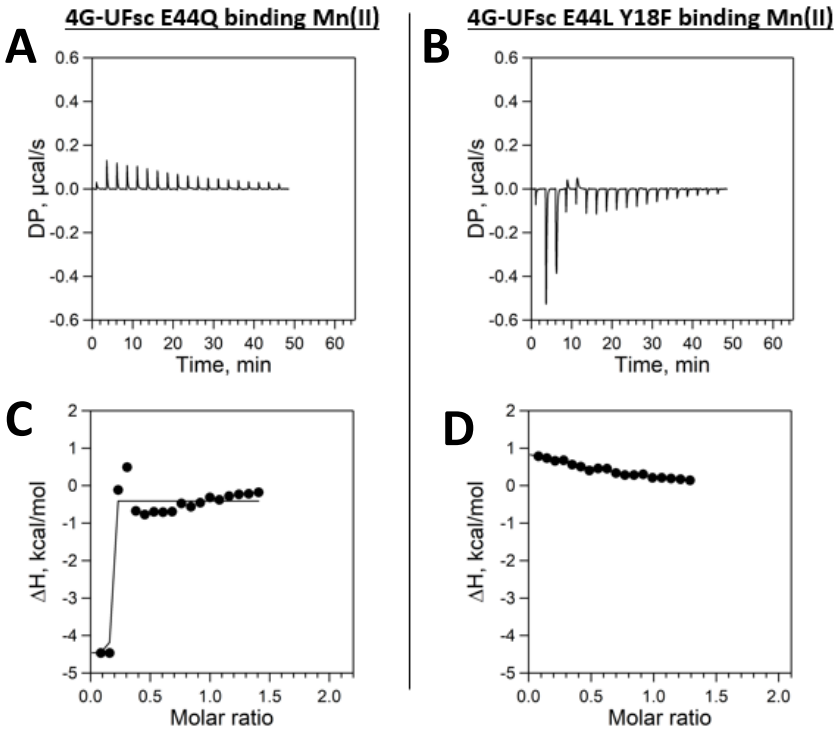

Figure 19: ITC analysis of 4G-UFsc E44 mutants binding to manganese (A) Thermogram of 4G-UFsc E44Q binding Mn(II) (B) Thermogram of UFsc E44L Y18F binding Mn(II) (C) Integrated binding isotherm of 4G-UFsc E44Q binding to Mn(II) (D) Integrated binding isotherm of 4G-UFsc E44Q binding to Mn(II).

Table 7. ITC thermodynamic parameters for 4G-UFsc, 4G-UFsc E44Q, and 4G-UFsc E44L Y18F binding to Mn(II).

Metal	Parameters	4G-UFsc	4G-UFsc E44Q	4G-UFsc E44L Y18F
Mn (II)	N	0.959	No binding	
	Kd, nM	9250		> 100 µM
	ΔH, kcal/mol	-2.57		

The integrated binding isotherm for 4G-UFsc E44Q does not show a binding curve(Figure 19C). This means that the mutant does not bind Mn(II). The parameters of the ITC analysis of 4G-UFsc E44L Y18F were inconclusive and the concentration of metal needs to be adjusted in order to produce a reliable binding curve.

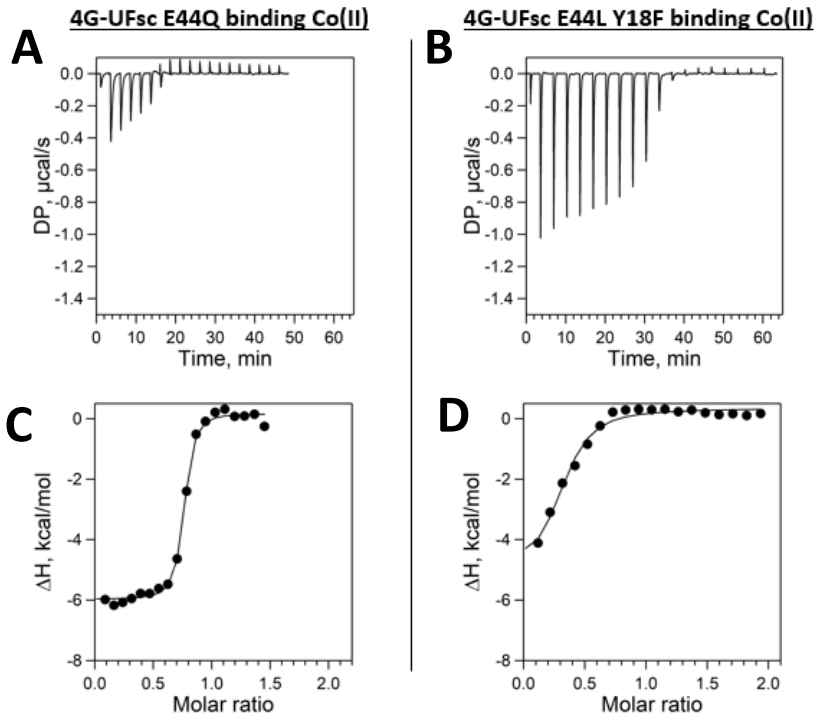

Figure 20: ITC analysis of 4G-UFsc E44 mutants binding to cobalt (A) Thermogram of 4G-UFsc E44Q binding Co(II) (B) Thermogram of UFsc E44L Y18F binding Co(II) (C) Integrated binding isotherm of 4G-UFsc E44Q binding to Co(II) (D) Integrated binding isotherm of 4G-UFsc E44Q binding to Co(II).

Table 8. ITC thermodynamic parameters for 4G-UFsc, 4G-UFsc E44Q, and 4G-UFsc E44L Y18F binding to Co(II).

Metal	Parameters	4G-UFsc	4G-UFsc E44Q	4G-UFsc E44L Y18F
Co (II)	N	0.836	0.707	0.319
	Kd, nM	67	231	7150
	ΔH, kcal/mol	-9.21	-6.16	-5.32

As evident in the integrated binding isotherms of 4G-UFsc E44Q and 4G-UFsc E44L Y18F (Figure 20C and Figure 20D), both mutants bind Co(II). The K_d values of the E44Q mutant and of the double mutant (E44L Y18F) are larger than the K_d value of 4G-UFsc (Table 8). This means that the equilibrium association constant for these mutants is lower, and that mutations introduced at position 44 of 4G-UFsc decreased the protein's affinity for Co(II). The double mutant drastically decreases the protein's affinity for Co(II).

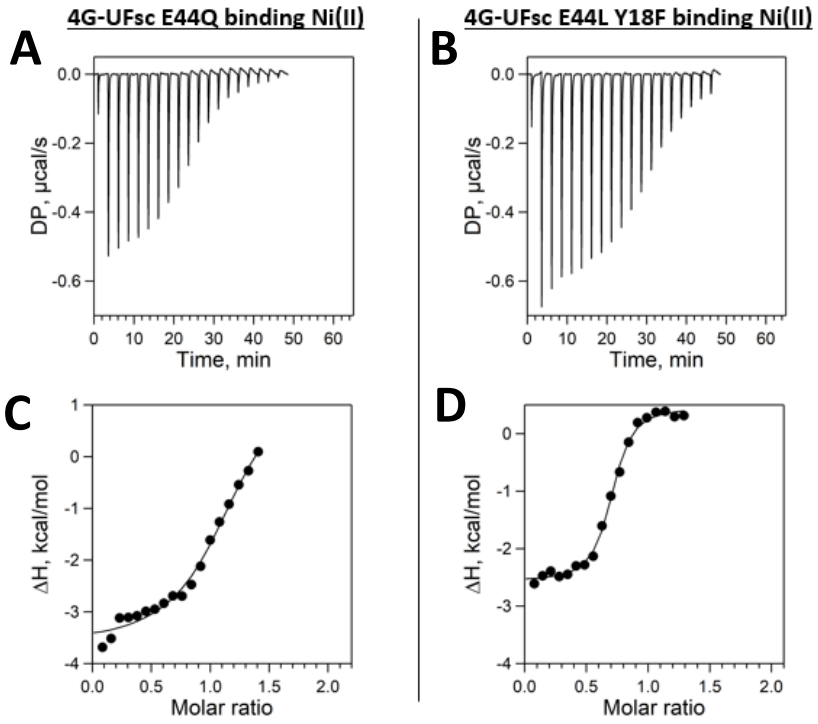

Figure 21: ITC analysis of 4G-UFsc E44 mutants binding to nickel (A) Thermogram of 4G-UFsc E44Q binding Ni(II) (B) Thermogram of UFsc E44L Y18F binding Ni(II) (C) Integrated binding isotherm of 4G-UFsc E44Q binding to Ni(II) (D) Integrated binding isotherm of 4G-UFsc E44Q binding to Ni(II).

Table 9. ITC thermodynamic parameters for 4G-UFsc, 4G-UFsc E44Q, and 4G-UFsc E44L Y18F binding to Ni(II).

Metal	Parameters	4G-UFsc	4G-UFsc E44Q	4G-UFsc E44L Y18F
Ni (II)	N	0.763	1.17	0.737
	Kd, nM	220	7180	1420
	ΔH, kcal/mol	-7.61	-5.12	-3.14

By looking at the values in Table 9, the K_d values for 4G-UFsc E44Q and 4G-UFsc E44L Y18F are higher than the K_d value of 4G-UFsc, meaning that these mutations decrease the protein's affinity for Ni(II). The E44Q mutation introduced to 4G-UFsc resulted in a higher K_d value than the double mutant (E44L Y18F), which means the introducing the single mutation at position 44 in 4G-UFsc decreased the protein's affinity for Ni(II) to a greater extent.

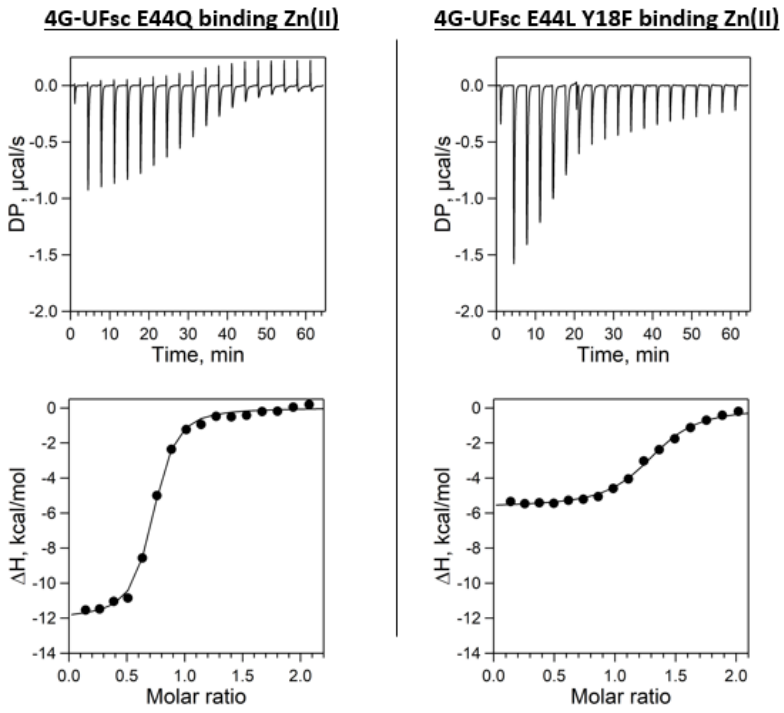

Figure 22: ITC analysis of 4G-UFsc E44 mutants binding to zinc obtained from the competition titration with TETA. (A) Thermogram of 4G-UFsc E44Q binding Zn(II) (B) Thermogram of 4G-UFsc E44L Y18F binding Zn(II) (C) Integrated binding isotherm of 4G-UFsc E44Q binding to Zn(II) (D) Integrated binding isotherm of 4G-UFsc E44Q binding to Zn(II).

Table 10. ITC thermodynamic parameters for 4G-UFsc, 4G-UFsc E44Q, and 4G-UFsc E44L Y18F binding to Zn(II).

Metal	Parameters	4G-UFsc	4G-UFsc E44Q	4G-UFsc E44L Y18F
Zn (II) (competition with TETA)	N	0.817	0.686	1.28
	Kd, nM	0.0302	1.11	2.43
	ΔH, kcal/mol	-12.00	-8.42	-2.05

By looking at the values in Table 10, the K_d values for 4G-UFsc E44Q and 4G-UFsc E44L Y18F are slightly higher than the K_d value of 4G-UFsc, meaning that these mutations decrease the protein's affinity for Zn(II).

3.3. Conclusions and Future Work

CD data of all mutants showed that introducing mutations at position 44 of UFsc and 4G-UFsc changed the degree of protein helicity and therefore changed the proteins' interactions with zinc. By using ITC, it was discovered that most mutations to the E44 position in the proteins (UFsc and 4G-UFsc) reduced the affinity of the proteins to metals. An exception is UFsc E44 mutants binding to cobalt. Based on ITC analysis, we found that UFsc E44Q and UFsc E44L Y18F have a higher affinity for cobalt than UFsc. Wildtype UFsc binds Ni(II) and so does UFsc double mutant E44L Y18F; however, UFsc E44Q does not bind nickel. Based on ITC, it seems as if the identity of E44Q is important for the protein to be able to bind Ni(II). Most of the mutations introduced lowered the proteins' affinity for metal ions but the extent by which the proteins' affinities were decreased was dependent on the mutant and on the identity of the metal.

Future work includes using CD and ITC to analyze the rest of the mutants our lab has created. Once those have been tested and the data has been organized and analyzed, more

mutations can be made to better understand coordination geometry and more metals can be tested.

3.4. Experimental

CD spectroscopy. On a Jasco J-715 CD spectrometer, CD spectra were obtained using a step scan averaging mode over 3 runs and a quartz cuvette with a 0.1 cm path length. Samples contained apo protein (20 μM) or metal-bound protein (20 μM protein and 200 μM $ZnCl_2$) in buffer (5 mM HEPES, pH 7.6). In order to assure reliable MRE values, the sample absorbance never exceed 1.5.

Isothermal Titration Calorimetry. As described in chapter 1 of this thesis, ITC was used to determine the binding stoichiometry (n) of proteins to ensure purity prior to running any experiments. In this portion of work described in chapter 3, ITC was used to monitor thermodynamic parameters of metal binding to UFsc and 4G-UFsc mutants. This was done using a MicroCal PEAQ-ITC instrument (Malvern). The exact concentration of protein was determined via UV-Vis spectroscopy. Stock solutions of metal salts (50 mM) were prepared in water and then diluted to the appropriate concentrations in buffer (25 mM HEPES, 100 mM NaCl, pH 7.6). The concentrations of the metal stock solutions used were confirmed by ICP-OES. The protein was placed in the calorimeter cell and was titrated wit metal solutions by automatic injections at 25˚C with 750 rpm stir speed. Microcal PEAQ-ITC Analysis software provided by the manufacturer performed baseline corrections and integrated peaks corresponding to each injection. The data was fitted to the one set of sites model for UFsc and 4G-UFsc mutants to

determine the stoichiometry (n), enthalpy of complex formation (ΔH), and equilibrium dissociation constant (K_d) parameters.

Additional Work

Preparation of Competent Cells

The preparation of competent cells begins with creating a small culture by scraping off a small amount of frozen BL21 commercial competent cells and adding it to 2 mL of LB. The culture is grown at 37˚C for 4 hours at 200 rpm. The starter culture is then diluted by adding it to 100 mL of autoclaved 2X LB. The culture is grow until OD_{600} = 0.55 at 18˚C, 200 rpm. This step takes about 5 hours. Once the OD_{600} = 0.55, the culture is transferred to ice and kept on ice for 10 minutes. The culture is then split into 2 sterile 50 mL falcon tubes and centrifuged at 2,500 g for 10 minutes at 4˚C. The supernatant is poured off and each pellet is re-dissolved in 30 mL of ice-cold Inoue buffer (12.5 mM HEPES pH 6.7, 68.7 mM $MnCl_2*4H_2O$, 18.7 mM $CaCl_2*2H_2O$, 0.3125 M KCl). After the pellet is resuspended in buffer, it is centrifuged at 2,500 g for 10 minutes at 4˚C. The buffer is removed following centrifugation and the falcon tubes are kept upside down for 5 minutes to allow the cells to completely dry. Once dried, the cells are resuspended in 8 mL of ice-cold Inoue buffer. 600 µL of DMSO are added and the solution is kept on ice for 10 minutes. 50 µL of solution are aliquoted into sterile chilled Eppendorf tubes. Liquid nitrogen is used to flash freeze the aliquots and they are then stored at -80˚C.

Peptide Synthesis

Our lab is collaborating with SBI to work on a project that involves materials changing properties in the presence of bacteria. The beginnings of this project involve short peptide

synthesis. My work on this project involved synthesizing the KK5 peptide. The sequence of the KK5 peptide is as follows: Ac-KGLAK-$CONH_2$. I also participated in precipitating the peptide via ether precipitation, which was later removed from the protocol in order to optimize KK5 synthesis by increasing yield.

The peptide was synthesized by manual fluorenylmethyloxycarbonyl (Fmoc) solid phase synthesis at elevated temperature (70˚C). Rink amide resin (ChemImpex International) was used as the solid support. Dimethylformanide (DMF) was used to swell the resin for 30 minutes and deprotection of the resin was done by using 5% piperazine in DMF for 5 minutes. The short linear peptide was synthesized from the C-terminus to the N-terminus. Each coupling consisted of (1) Fmoc-deprotection with 5% piperazine in DMF for 5 minutes, (2) washing 4 times with DMF, (3) coupling of the amino acid n the presence of HCTU and DIEA, and (4) washing with DMF twice. This procedure was repeated for coupling of next amino acid in the sequence.

Cleavage of the peptide from the resin and side chain deprotection was achieved by treatment with a mixture of trifluoroacetic acid for two hours at room temperature. The crude peptide was precipitated and washed with cold methyl *tert*-Butyl ether. Although I was unable to participate in the purification of the peptide I created, the post-doctorate that I was working under for this project purified my peptide on a preparative reverse phase HPLC system (Varian ProsStar 210). Dr. Areetha D'Souza lyophilized the KK5 peptide I synthesized and confirmed the identity of the peptide via MALDI-TOF mass spectrometry (Bruker Autoflex III Smartbeam MALDI-TOF mass spectrometer). The MALDI-TOF spectrometry of the KK5 peptide I synthesized is shown in the figure below.

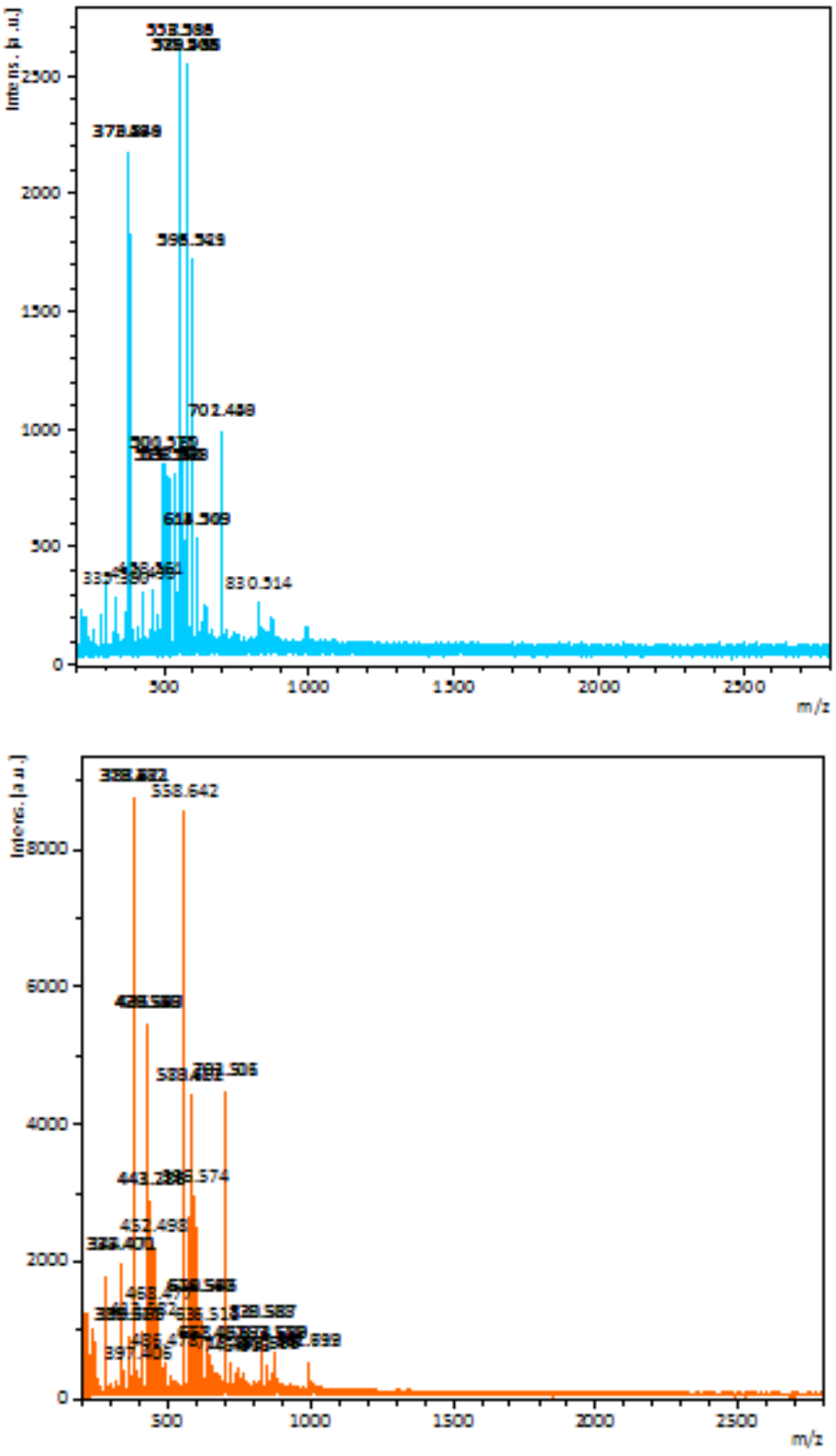

Figure 23. MALDI results from Dr. D'Souza of the KK5 peptide I synthesized.

References

1. Reig, A. J. *et al.* Alteration of the oxygen-dependent reactivity of de novo Due Ferri proteins. *Nat. Chem.* **4**, 900–906 (2012).

2. Ulas, G., Lemmin, T., Wu, Y., Gassner, G. T. & DeGrado, W. F. Designed metalloprotein stabilizes a semiquinone radical. *Nat. Chem.* **8**, 354–359 (2016).

3. Yoon, J. H., Kulesha, A. V, Lengyel-zhand, Z. & Volkov, A. N. Uno Ferro , a de Novo Designed Protein , Binds Transition Metals with High Affinity and Stabilizes Semiquinone Radical Anion. *Chem. Eur. J.* 1–6 (2019). doi:10.1002/chem.201904020

4. Carter, E. L. *et al.* Interplay of metal ions and urease. *Metallomics* 207–221 (2009). doi:10.1039/b903311d

5. Valdez, C. E. & Alexandrova, A. N. Why Urease Is a Di-Nickel Enzyme whereas the CcrA β -Lactamase Is a Di-Zinc Enzyme. *J. Phys. Chem.* (2012). doi:10.1021/jp302771n

6. Calhoun, J. R. *et al.* Artificial Diiron Proteins : From Structure to Function †. *Pept. Sci.* 1–3 doi:10.1002/bip.20230

7. Calhoun, J. R. *et al.* Computational Design and Characterization of a Monomeric Helical Dinuclear Metalloprotein. *J. Mol. Biol.* 1101–1115 (2003). doi:10.1016/j.jmb.2003.10.004

8. Costanzo, L. Di *et al.* Toward the de Novo Design of a Catalytically Active Helix Bundle : A Substrate-Accessible Carboxylate-Bridged Dinuclear Metal Center. *J. Am. Chem. Soc.* 6298–6305 (2001).

9. Martı, E., Ca, F. J., Zorrilla, S. & Pe, D. Drawbacks of Dialysis Procedures for Removal of EDTA. *PLoS One* 1–9 (2017). doi:10.1371/journal.pone.0169843

10. He, Q., Mason, A. B. & Woodworth, R. C. Spectrophotometric titration with cobalt(III) for the determination of accurate absorption coefficients of transferrins. *Biochem. J.* **148**, 145–148 (1996).

11. Singh, S. & Hider, R. C. *Therapeutic iron-chelating agents*. *New Comprehensive Biochemistry* **28**, (Elsevier Science B.V., 1994).

12. Lee, D. & Lippard, S. J. Nonheme Di-iron Enzymes. 10–13